patients with IL-12p40 and IL-12Rβ1 deficiencies, which impair IFN-γ immunity in all patients and IL-17A/F immunity in some patients (*4*). We studied seven patients from three unrelated consanguineous families with this unusual combination of infectious diseases but no known genetic disorder. A Palestinian child (Fig. 1A, Kindred A, patient P1; see also supplementary text) died at the age of 6 years from disseminated BCG disease. Two other children (P2 and P3) in Kindred A had similar clinical presentations but survived and are now 7 and 4 years old, respectively. A 6-year-old Chilean child (Fig. 1A, Kindred B, P4; see also supplementary text) had disseminated BCG infection at age 16 months. Finally, three siblings from Saudi Arabia (Fig. 1A, Kindred C, P5, P6, and P7; see also supplementary text), ages 9, 6, and 3 years, had mycobacterial diseases caused by BCG in two children and by *M. tuberculosis* in the third. Six of the seven patients also had mucocutaneous candidiasis of varying severity (table S1).

Bi-allelic *RORC* mutations

We combined whole-exome sequencing and genome-wide linkage (GWL) analysis to search for homozygous genetic lesions in the three probands (P1, P4, and P6) (fig. S1). We identified a homozygous C/T mutation in the *RORC* gene in P1, P2, and P3, resulting in a missense Ser^{38}→Leu^{38} (S38L) substitution in the RORγ isoform or a S17L substitution in the RORγT isoform (Fig. 1, A and B, and fig. S2). In P4, we identified a homozygous *RORC* C/T mutation converting the Gln^{329} (Q329) residue of RORγ (or Q308 in RORγT) into a stop codon (Fig. 1, A and B, and fig. S2). In P5, P6, and P7, we identified a homozygous C/T mutation converting the Q441 residue of RORγ (or Q420 in RORγT) into a stop codon (Fig. 1, A and B, and fig. S2). In each kindred, all unaffected family members were either heterozygous or homozygous for the wild-type (WT) allele (Fig. 1A and fig. S2). The familial segregation of these mutant *RORC* alleles was therefore consistent with an autosomal recessive (AR) pattern of inheritance. There were no other genes mutated in the three kindreds among the 173 genes on the 6.87-Mb interval linked with disease (maximum LOD score 6.35). The S17L mutation affects a strictly conserved residue of the DNA binding domain of RORγT (Fig. 1B) and is predicted to be damaging by multiple software algorithms (*5*). The Q308X and Q420X (X signifies a stop codon) nonsense mutations are predicted to result in truncated proteins lacking part of the ligand-binding domain (Fig. 1B). The Q308X and Q420X alleles were not found in the National Center for Biotechnology Information, Ensembl, Exome Aggregation Consortium (ExAC), and dbSNP databases; in our own in-house database of more than 3000 exomes; or in 1052 controls from 52 ethnic groups in the CEPH-HGD panel, indicating that they were very rare variants, possibly exclusive to these two kindreds. There were no nonsense or frameshift mutations affecting isoform 2 (RORγT) in these databases. The S17L allele was found in one heterozygous individual of the ExAC database, indicating that its frequency is less than 10^{-5}. We therefore hypothesized that the bi-allelic *RORC* mutations found in these three kindreds were disease-causing.

Complete RORγ and RORγT deficiency

In mice and humans, the RORγ and RORγT isoforms are generated by transcription from different start sites (*6*–*10*) (Fig. 1B). Both molecules are transcription factors, but they have different expression patterns in inbred mice: RORγ is ubiquitous, whereas RORγT is restricted to leukocytes (*10*). RORγT plays an important role in T cell development and function in mice (*11*, *12*). Animals lacking only RORγT apparently have the same immunological phenotype as those lacking both isoforms (*10*). We first assessed the effect of *RORC* mutations by transiently expressing WT and mutant RORγT and RORγ in human embryonic kidney 293T (HEK293T) cells in the presence and absence of stimulation with phorbol 12-myristate 13-acetate (PMA) and ionomycin. We detected both the WT and S17L RORγT proteins at the expected molecular mass of 56 kD (Fig. 1C). The Q308X and Q420X RORγT mutant proteins had molecular weights consistent with truncation at residues 308 and 420, respectively (Fig. 1C). Similar results were obtained upon expression of RORγ (fig. S3). We then performed an electrophoretic mobility shift assay (EMSA) to assess the ability of the mutant RORγT and RORγ isoforms to respectively bind to RORE-2 and RORE-1, the consensus binding sites in the promoter of *IL17A* (fig. S3). The three mutations abolished DNA binding of RORγT to RORE-2 (Fig. 1C) and of RORγ to RORE-1 (fig. S3), but not by disrupting the nuclear localization of the protein (fig. S3). Each mutation resulted in the loss of *IL17A* promoter activation by RORγT (Fig. 1D) or RORγ (fig. S4). Thus, each mutant allele was associated with a complete loss of function of the two encoded protein isoforms, identifying these patients as cases of human AR complete RORγ/RORγT deficiency (hereafter referred to as RORγT deficiency).

Broad immunological phenotype

Mouse RORγT is expressed in lymphoid tissue inducer (LTi) cells, type 3 innate lymphoid cells (ILC3), type 1 natural killer T (NKT) cells, some γδ T cells, immature $CD4^+CD8^+$ αβ thymocytes, and IL-17A/F–producing $CD4^+$ αβ T cells [T helper 17 (T_H17) cells] (*7*, *11*, *13*–*16*). LTi, ILC3, type 1 NKT, and T_H17 cells fail to develop in $Rorc^{-/-}$ mice, and $CD4^+CD8^+$ αβ thymocytes have a reduced life span (*11*, *14*, *17*). $RORC^{-/-}$ patients displayed clinical signs consistent with LTi deficiency, including absence of palpable axillary and cervical lymph nodes (despite visible tonsils), and had reduced thymus size (Fig. 2A). As in $Rorc^{-/-}$ mice, ILC3 were barely detectable in the patients' blood (fig. S5). In $Rorc^{-/-}$ mice, the short life span of $CD4^+CD8^+$ αβ thymocytes results in an inability to use the most 5′ segments of the T cell receptor (TCR) Vα array (*12*), including those encoding the Vα chains of mucosal associated invariant T (MAIT) (*12*) and type 1 NKT cells (*18*). High-throughput sequencing of the *TRA/TRD* and *TRG* loci revealed that 5′ Vα gene segment use had decreased, whereas Vδ and Vγ usage was normal in $RORC^{-/-}$ T cell clonotypes (fig. S6). Further, these patients lacked *TRA* clonotypes using 5′ Vα and distal 3′ Jα pairings (fig. S6). In total $RORC^{-/-}$ T cell clonotypes, the usage of Vγ9 was elevated (fig. S6), consistent with antigen-driven peripheral expansion of this subset, perhaps driven by mycobacteria (*19*). Abolished use of the Vα segments *TRAV10* (encoding Vα24) and *TRAV1.2* (encoding Vα7.2) was confirmed by quantitative polymerase chain reaction

[1]St. Giles Laboratory of Human Genetics of Infectious Diseases, Rockefeller Branch, The Rockefeller University, New York, NY 10065, USA. [2]Department of Pediatrics, Hiroshima University Graduate School of Biomedical and Health Sciences, Hiroshima, Japan. [3]Immunology Division, Garvan Institute of Medical Research, Darlinghurst, New South Wales, Australia. [4]St Vincent's Clinical School, University of New South Wales, Sydney, New South Wales, Australia. [5]Institute for Research in Biomedicine, University of Italian Switzerland, Bellinzona, Switzerland. [6]Department of Pediatrics, Hadassah University Hospital, Jerusalem, Israel. [7]Department of Immunology, School of Medicine, Universidad de Valparaíso, Santiago, Chile. [8]Department of Pediatrics, Padre Hurtado Hospital and Clinica Alemana, Santiago, Chile. [9]Department of Pediatrics, King Faisal Specialist Hospital and Research Center, Riyadh, Saudi Arabia. [10]Department of Pediatrics, Prince Naif Center for Immunology Research, College of Medicine, King Saud University, Riyadh, Saudi Arabia. [11]Institut Curie, INSERM U932, Paris, France. [12]Division of Immunology, Boston Children's Hospital, Boston, MA 02115, USA. [13]Caritas Baby Hospital, Post Office Box 11535, Jerusalem, Israel. [14]Laboratory of Human Genetics of Infectious Diseases, Necker Branch, INSERM UMR 1163, Paris, France. [15]Paris Descartes University, Imagine Institute, Paris, France. [16]Trudeau Institute, Saranac Lake, NY 12983, USA. [17]La Jolla Institute for Allergy and Immunology, La Jolla, CA 92037, USA. [18]Department of Radiology, Assistance Publique–Hôpitaux de Paris (AP-HP), Necker Hospital for Sick Children, Paris, France. [19]Department of Microbiology and Immunology, Peter Doherty Institute for Infection and Immunity, University of Melbourne, Parkville, Victoria, Australia. [20]Department of Biochemistry and Molecular Biology, School of Biomedical Sciences, Monash University, Clayton, Victoria, Australia. [21]Australian Research Council Centre of Excellence for Advanced Molecular Imaging, Monash University, Clayton, Victoria, Australia. [22]Institute of Infection and Immunity, Cardiff University, School of Medicine, Heath Park, Cardiff CF14 4XN, UK. [23]Laboratoire Dynamique du Génome et Système Immunitaire, INSERM UMR 1163, Université Paris Descartes–Sorbonne Paris Cité, Imagine Institute, Paris, France. [24]Pediatric Hematology-Immunology Unit, AP-HP, Necker Hospital for Sick Children, Paris, France. [25]Institute of Cellular Medicine, Newcastle University and Great North Children's Hospital, Newcastle upon Tyne NE4 6BE, UK. [26]Laboratory of Lymphocyte Activation and Susceptibility to EBV Infection, INSERM UMR 1163, Université Paris Descartes–Sorbonne Paris Cité, Imagine Institute, Paris, France. [27]Department of Paediatric Allergy Immunology, University of Manchester, Royal Manchester Children's Hospital, Manchester, UK. [28]Center for the Study of Primary Immunodeficiencies, AP-HP, Necker Hospital for Sick Children, Paris, France. [29]Manton Center for Orphan Disease Research, Children's Hospital, Boston, MA 02115, USA. [30]Center of Medical Immunology, Institute for Research in Biomedicine, University of Italian Switzerland, Bellinzona, Switzerland. [31]Howard Hughes Medical Institute, New York, NY 10065, USA.

*These authors contributed equally to this work. **†Corresponding author. E-mail: jmarkle@rockefeller.edu (J.G.M.); jean-laurent.casanova@rockefeller.edu (J.-L.C.)** ‡These authors contributed equally to this work. §Present address: Life and Health Sciences Research Institute (ICVS), School of Health Sciences, University of Minho, Braga, Portugal. ||Present address: National Center for HIV/AIDS, Viral Hepatitis, STD, and TB Prevention, Office of Infectious Diseases, Centers for Disease Control and Prevention, Atlanta, GA 30329, USA. ¶These authors contributed equally to this work. #These authors contributed equally to this work.

(fig. S7) and resulted in a lack of both CD161$^+$Vα7.2$^+$ MAIT cells and Vα24$^+$Vβ11$^+$ type 1 NKT cells (Fig. 2, B and C, and fig. S7). Some Vα7.2$^+$ cells other than MAIT cells have recently been shown to recognize *Mycobacterium*-derived mycolyl lipids (*20*); they were also missing in *RORC*$^{-/-}$ patients. Nevertheless, *RORC*$^{-/-}$ patients displayed only mild CD4$^+$ and CD8$^+$ αβ T cell lymphopenia, with normal B and NK cell counts (Fig. 2D and table S2). These patients did not, therefore, have T cell deficiency [also known as "combined" immunodeficiency (CID)], consistent with their lack of broad infectious and autoimmune phenotypes (*21*). Finally, the frequencies of circulating γδ T cells were normal (table S2). Overall, these *RORC*$^{-/-}$ patients displayed the general immunological features characteristic of *Rorc*$^{-/-}$ mice (*11, 12, 14, 22, 23*). These studies also revealed that the development of MAIT and other Vα7.2$^+$ T cells is critically dependent on RORγT, which had been predicted but not shown in mice. No infectious phenotype can be unambiguously assigned to any of these individual immunological anomalies.

Abolished production of IL-17A/F

Given the critical role of murine RORγT in generating IL-17A/F– and IL-22–producing lymphocytes [including ILC3, γδ T cells, and T_H17 cells (*11, 13, 24*)] and the finding that patients with compromised IL-17A/F immunity are susceptible to mucocutaneous candidiasis (*1*), we assessed the development and function of IL-17A/F–producing lymphocytes in the patients. Circulating ILC3 were too few to assess their production of IL-17. CD3$^+$ T cells from *RORC*$^{-/-}$ patients displayed a severe impairment in the production of IL-17A, IL-17F, and IL-22, at both the mRNA (fig. S8) and the protein level (Fig. 3A), after polyclonal stimulation. CD4$^+$ αβ T cells are a major source of IL-17A/F (*9*). Memory (CD45RA$^-$) CD4$^+$ T cells from *RORC*$^{-/-}$ patients produced much less IL-17A, IL-17F, and IL-22 than WT and heterozygous controls (Fig. 3B).

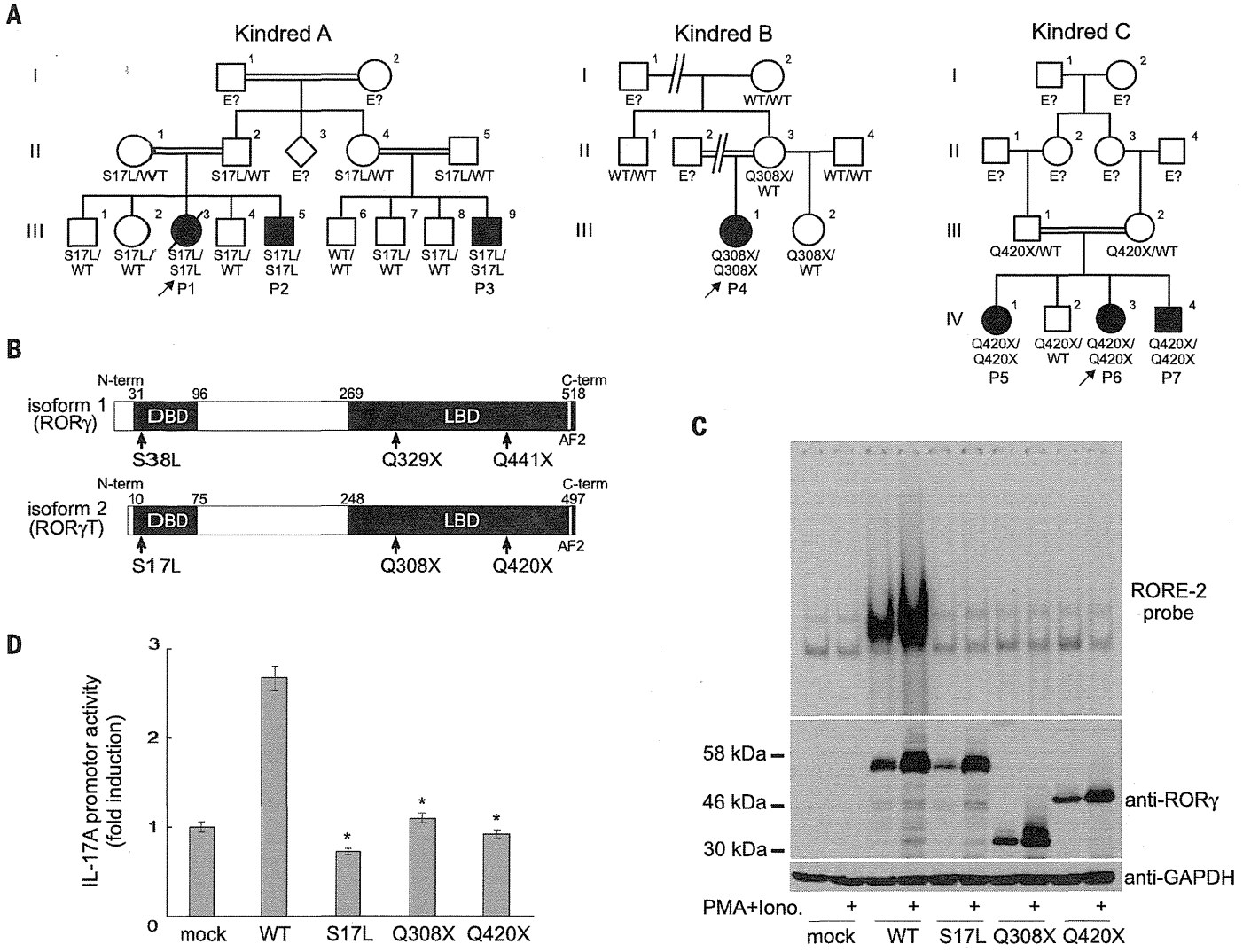

Fig. 1. Identification of homozygous loss-of-function mutations affecting the human RORγT protein. (**A**) Sanger sequencing results and familial segregation of previously unidentified homozygous *RORC* mutations in three unrelated consanguineous families, indicating an AR pattern of inheritance, with complete clinical penetrance. P1, patient 1; P2, patient 2; etc. (**B**) Graphical representation of the RORγ and RORγT proteins, encoded by *RORC* isoforms 1 and 2, respectively. AF2, activation function 2 domain. Arrows indicate the location of the sites affected by the *RORC* mutations found in the families. DBD, DNA binding domain; LBD, ligand-binding domain. (**C**) HEK293T cells were either mock-transfected or transfected with the indicated plasmids. After 24 hours, cells were either left untreated or stimulated with PMA and ionomycin. Whole-cell lysates were obtained and subjected to Western blotting (lower panel), and nuclear lysates were subjected to EMSA with a ^{32}P-labeled RORE-2 probe derived from the *IL17A* promoter sequence (upper panel). GAPDH, glyceraldehyde-3-phosphate dehydrogenase. (**D**) *IL17A* reporter plasmids, the pRL-SV40 vector, and WT or mutant *RORC* plasmid were used to transfect HEK293T cells. After 24 hours, cells were stimulated with PMA and ionomycin as in (C) and then subjected to luciferase assays. Experiments were performed in triplicate, and *IL17A* promoter activity is expressed as fold induction relative to mock-transfected cells. *P < 0.05 versus WT controls; two-tailed Mann-Whitney tests with Bonferroni correction. Error bars denote SEM.

In contrast, the memory CD4$^+$ T cells from these patients produced large amounts of IL-4, IL-5, and IL-13 (fig. S8). In separate experiments, naïve (CD45RA$^+$CCR7$^+$) CD4$^+$ T cells from *RORC*$^{-/-}$ patients cultured under T_H17-polarizing conditions secreted less IL-17A and IL-17F than cells from healthy donors or heterozygous relatives (Fig. 3C). We next assessed the proliferation and cytokine secretion of highly purified WT, heterozygous, and *RORC*$^{-/-}$ CD4$^+$CCR6$^+$ memory αβ T cells (fig. S9), a population enriched in IL-17A/F-secreting cells (T_H17 cells, which express CCR4), as well as cells secreting IL-17A/F and IFN-γ (herein designated as T_H1^* cells, which express CXCR3) (*25*), after stimulation with *C. albicans* lysate. By monitoring the incorporation of a radioactive label, we found that CD4$^+$CCR6$^+$ T cells from *RORC*$^{-/-}$ patients had normal frequencies of antigen-specific cells recognizing *C. albicans* (Fig. 3D). However, these cells [including both T_H17 and T_H1^* cells, whose proportions were normal (fig. S9)] secreted much lower amounts of IL-17A and IL-22 than did control cells (Fig. 3E). IFN-γ was also reduced, but large amounts of IL-4 were secreted, serving as a control (Fig. 3E). Finally, *Herpesvirus saimiri*–transformed CD4$^+$ αβ T cells from *RORC*$^{-/-}$ patients showed abolished induction of *RORC* (Fig. 4A) and *IL17A* (Fig. 4B), but not *IFNG* serving as a control (fig. S10). The defect in *IL17A* induction could be rescued by retroviral transduction with WT *RORC* (Fig. 4B). Collectively, these data demonstrate a profound diminution of IL-17A/F and IL-22 production by all leukocytes tested in *RORC*$^{-/-}$ patients. As CMC-causing germline mutations have previously been identified in *IL17F*, *IL17RA*, *IL17RC*, and *ACT1* (*1*, *2*, *26*), we conclude that impaired IL-17A/F immunity in *RORC*$^{-/-}$ patients accounts for their development of CMC. Human IL-17A/F–producing ILC3, γδ T cells, and αβ T cells, or any of their subsets, may individually or collectively confer protection against *Candida*.

Selective defect in IFN-γ production

We then investigated the cellular mechanism underlying the patients' surprising susceptibility to mycobacteria. The patients did not display chronic granulomatous disease or severe CID, which can underlie BCG disease (*4*). The CD3$^+$ T cells (including both γδ and αβ T cells) from *RORC*$^{-/-}$ patients produced IFN-γ normally, after the stimulation of whole blood or peripheral blood mononuclear cells (PBMCs) with PMA and ionomycin (fig. S10). Likewise, total CD4$^+$ αβ T cells, memory (CD45RA$^-$) CD4$^+$ T cells, naïve CD4$^+$ T cells cultured under T_H1-polarizing conditions, and *Herpesvirus saimiri*–transformed T cells from

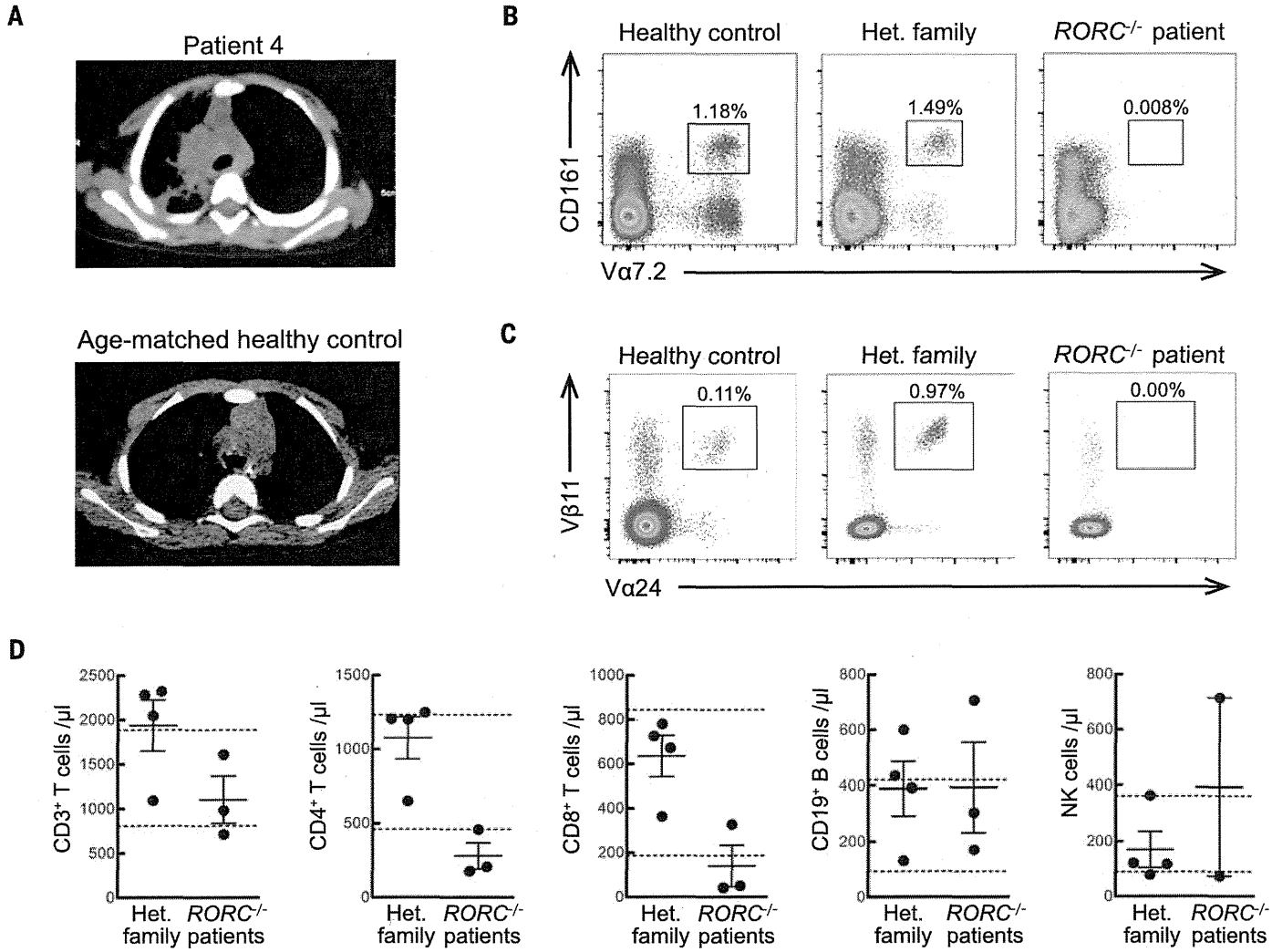

Fig. 2. *RORC*$^{-/-}$ patients display abnormal thymus size and TCRα rearrangement in line with their mild T cell lymphopenia with a complete absence of MAIT and type 1 NKT cells. (**A**) Computed tomography (CT) scan of P4's chest at the age of 16 months compared with a CT scan of a healthy control. P4's scan reveals right lung infiltrate and thymic hypoplasia. (**B** and **C**) PBMCs from WT controls, heterozygous family members, or *RORC*$^{-/-}$ patients were analyzed for MAIT (B) and type 1 NKT (C) cell frequencies by flow cytometry. Each plot is representative of $n = 3$ experiments. (**D**) Cell counts were performed on fresh blood samples from heterozygous family members ($n = 4$) and *RORC*$^{-/-}$ patients ($n = 3$). Dotted lines indicate the normal ranges for each lymphocyte population per microliter of blood, based on the results for healthy individuals tested at the Necker Hospital for Sick Children (Paris, France).

the patients produced IFN-γ normally (fig. S10). Overall, and in contrast to the IL-17A/F defect, RORγT deficiency does not impair IFN-γ secretion in conditions of polyclonal stimulation. We next assessed *Mycobacterium*-specific IFN-γ responses from whole blood (Fig. 5A) or PBMCs (Fig. 5B) of $RORC^{-/-}$ patients, heterozygous family members, and healthy controls. The patients' cells produced very little IFN-γ in response to treatment with BCG plus IL-12 (Fig. 5, A and B). This defect was as profound as that seen in patients with IL-12Rβ1 deficiency (*27*). The production of IL-12p40 by $RORC^{-/-}$ cells was normal (fig. S11). Impaired IFN-γ production may account for mycobacterial diseases in $RORC^{-/-}$ patients. This IFN-γ defect was not secondary to excessive IL-4, IL-5, or IL-13 production (fig. S11) or to the IL-17A/F defect (fig. S12). Many single-gene immunodeficiencies do not predispose to BCG disease despite impaired or abolished development or function of various αβ T cell subsets, including $CD4^+$ T cells (*28*), $CD8^+$ T cells (*29*), type 1 NKT cells (*30*, *31*), and MAIT cells (*31*). Even rare patients deficient in total αβ T cell function [$ZAP70^{-/-}$ (*32*), $TRAC^{-/-}$ (*33*)] have not been reported to develop BCG disease. Whole blood or PBMCs from such patients responded normally to treatment with BCG plus IL-12, except for patients lacking all functional αβ T cells (fig. S12). As MAIT cells were shown to respond to mycobacteria (*34*), we purified these

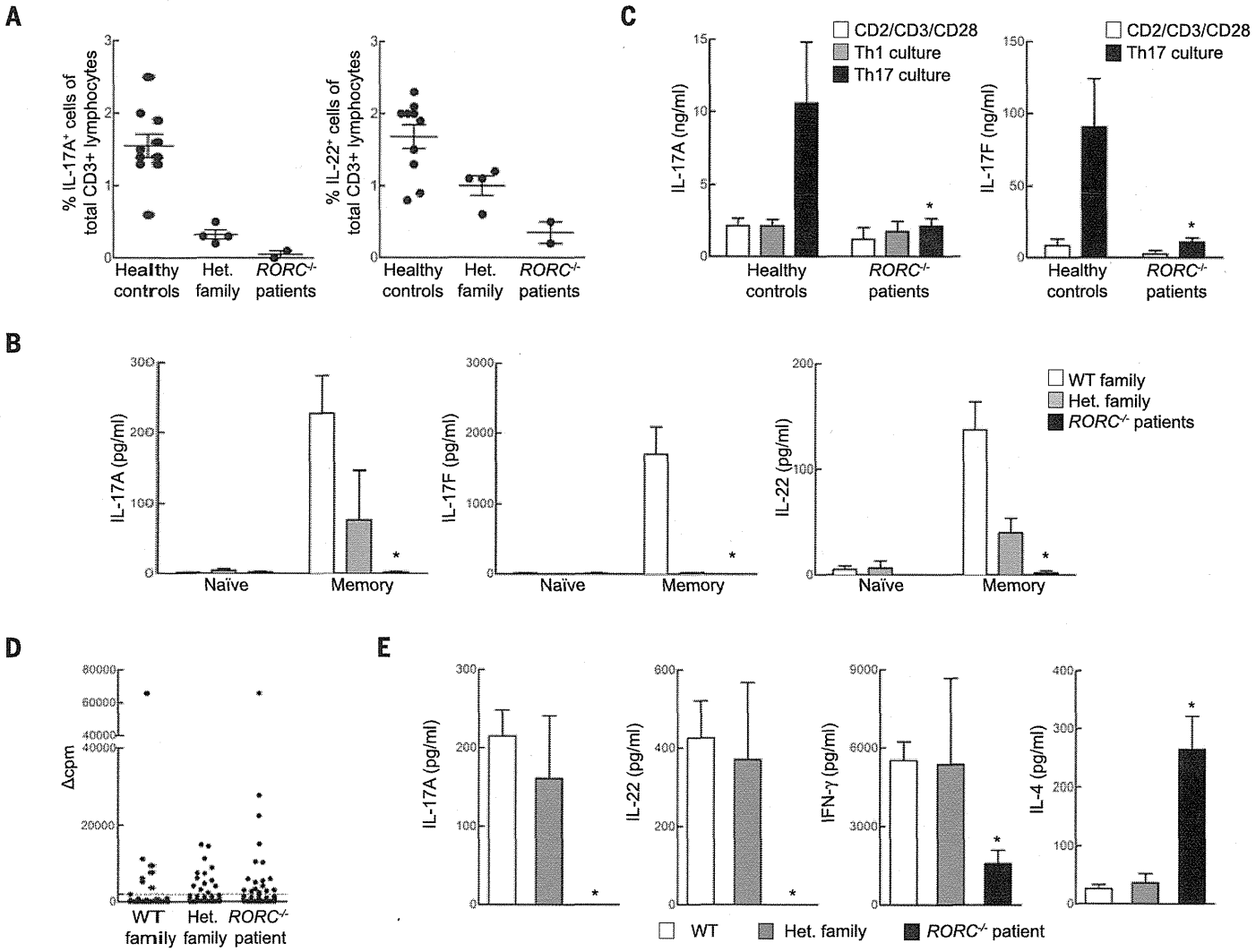

Fig. 3. Cellular mechanisms of compromised IL-17 immunity and CMC in $RORC^{-/-}$ patients. (**A**) Whole blood from healthy WT donors, heterozygous family members, or $RORC^{-/-}$ patients was activated by PMA and ionomycin in the presence of brefeldin A, then assessed by intracellular flow cytometry for the production of IL-17A and IL-22. (**B**) Naïve and memory $CD4^+$ T cells from WT controls ($n = 7$), heterozygous family members ($n = 2$), and $RORC^{-/-}$ patients ($n = 3$) were cultured with T cell activation and expansion (TAE) beads, and the culture supernatants were then assessed for secretion of the cytokine indicated (*37*). (**C**) Cytokine production by in vitro–differentiated $CD4^+$ T cells from control donors and $RORC^{-/-}$ patients. Naïve ($CD45RA^+CCR7^+$) $CD4^+$ T cells were purified from the PBMCs of WT controls ($n = 6$) or $RORC^{-/-}$ patients ($n = 3$), then cultured in the presence of TAE beads alone or TAE beads together with polarizing stimuli to induce the differentiation of T_H1- or T_H17-type cells (*37*). After 5 days, culture supernatants were assessed for the secretion of the cytokines indicated. (**D**) Sorted $CCR6^+$ memory $CD4^+$ T cells from WT controls, heterozygous family members, and $RORC^{-/-}$ patients were initially polyclonally stimulated to generate T cell libraries, then cultured with autologous irradiated B cells, with or without a 3-hour pulse with *C. albicans* lysate (5 μg/ml) (*37*). Proliferation was assessed by evaluating radiolabel incorporation on day 4 and is expressed as Δcpm values (cpm, counts per minute) (*37*). Dotted lines represent the cutoff values. The frequencies of specific T cells using the Poisson distribution were $315/10^6$, $631/10^6$, and $874/10^6$ in WT control, heterozygous family member, and $RORC^{-/-}$ patient, respectively. (**E**) Concentrations of the indicated cytokines were measured in the supernatants from positive cultures (Δcpm values above the cut-off value) from experiments performed as in (D) with cells from WT controls, heterozygous family members, and $RORC^{-/-}$ patients ($n = 2$ each). Number of wells: $n = 45$ to 64 for WT controls, $n = 4$ to 10 for heterozygous family members, and $n = 14$ to 23 for $RORC^{-/-}$ patients. *$P <$ 0.05 versus WT controls; in two-tailed Mann-Whitney tests with Bonferroni correction. Error bars in (B), (C), and (E) indicate SEM.

cells from WT donor PBMCs and added them to PBMCs from *RORC*$^{-/-}$ patients before BCG stimulation. The lack of MAIT cells in *RORC*$^{-/-}$ patients did not account for their impaired IFN-γ production (fig. S13). Overall, the absence of type 1 NKT and MAIT cells, the mild T cell lymphopenia, and the poor development of IL-17A/F T cells may contribute marginally to mycobacterial susceptibility but do not account for the low level of IFN-γ production by *RORC*$^{-/-}$ leukocytes stimulated with BCG and IL-12, and probably not for the patients' mycobacterial disease.

Impaired IFN-γ production by γδ T cells

We thus systematically characterized the consequences of leukocyte population depletions on BCG-dependent IFN-γ production by PBMCs in healthy controls. We found no overt IFN-γ defect as a consequence of depleting NK cells, CD14$^+$ cells, or CD4$^+$ or CD8$^+$ T cells. Depletion of αβ T cells, γδ T cells, or both resulted in diminished IFN-γ production (fig. S14). To probe the kinetics of this phenotype, a similar experiment was repeated and supernatant was assessed at 6, 12, 18, 24, and 48 hours poststimulation (fig. S14). The effect of γδ T cell depletion was most apparent at 24 hours (fig. S14). We observed high expression of *RORC* isoform 2 mRNA in both αβ and γδ T cells of healthy donors (fig. S15), prompting further analyses of γδ T cell function. Flow cytometry analyses revealed that the TCR^{high} γδ T cells from *RORC*$^{-/-}$ patients could not secrete IFN-γ in response to stimulation with PMA and ionomycin, unlike TCR^{low} γδ T cells (fig. S15). TCR Vδ2$^+$ cells have been reported as the predominant cells responding to human BCG vaccination (*19*). *RORC*$^{-/-}$ patients had normal frequencies of TCR Vδ2$^+$ cells, but these cells were unable to secrete IFN-γ when stimulated with PMA and ionomycin (fig. S15), suggesting a possible contribution of this γδ T cell subset defect to mycobacterial susceptibility in *RORC*$^{-/-}$ patients. Overall, RORγT deficiency diminishes the IFN-γ–producing capacity of γδ T cells, which normally produce this cytokine in response to *Mycobacterium* stimulation.

The patients' CD4$^+$CCR6$^+$ αβ T cells produce little IFN-γ in response to BCG

Previous studies have demonstrated that the T-bet– and RORγT-expressing, IFN-γ and IL-17A/F-producing CCR6$^+$CXCR3$^+$ T$_H$1* subset is strongly enriched for *Mycobacterium*-responsive CD4$^+$ αβ T cells, unlike the CCR6$^+$CCR4$^+$ T$_H$17 cells that only express RORγT and produce IL-17A/F and are enriched for *Candida*-responsive T cells (*25*). We therefore purified memory (CD45RA$^-$) αβ T cell subsets (fig. S9) and assessed their proliferation and cytokine production in response to a pool of BCG peptides. CD4$^+$CCR6$^+$ αβ T cells from *RORC*$^{-/-}$ patients had a normal or high frequency of antigen-specific cells recognizing BCG peptides, as demonstrated by the induction of proliferation (Fig. 5C and fig. S16). However, although CD4$^+$CCR6$^+$ T cells from *RORC*$^{-/-}$ patients responded to mycobacterial antigens, they secreted much less IFN-γ than CD4$^+$CCR6$^+$ αβ T cells from normal donors (Fig. 5D). The normal proliferation and cytokine production of other CD4$^+$ memory T cell subsets in response to *Candida* and *Mycobacterium* (fig. S17) and to irrelevant viral stimuli (fig. S18) indicate a selective RORγT-dependent functional defect in *Mycobacterium*-specific CD4$^+$CCR6$^+$ αβ T cells. Although we did not purify and test T$_H$1* cells, they were present in normal proportions in the patients (fig. S9), implying that they are functionally defective for IFN-γ production upon *Mycobacterium* stimulation. Collectively, these data suggest that mycobacterial diseases in *RORC*$^{-/-}$ patients may result from the poor production of IFN-γ by γδ T cells, CCR6$^+$CXCR3$^+$CD4$^+$ αβ T$_H$1* cells, or both in response to mycobacteria. IFN-γ treatment may therefore be beneficial for *RORC*$^{-/-}$ patients. This combined defect probably also accounts for mycobacterial disease in severe combined immunodeficient patients, as patients with various forms of CID are normally resistant to BCG (*27*, *33*). Finally, the lack of MAIT and type 1 NKT cells, reduction in ILC3, and possibly the absence of other lymphocytes not analyzed using blood samples (e.g., LTi) may aggravate the mycobacterial phenotype of *RORC*$^{-/-}$ patients.

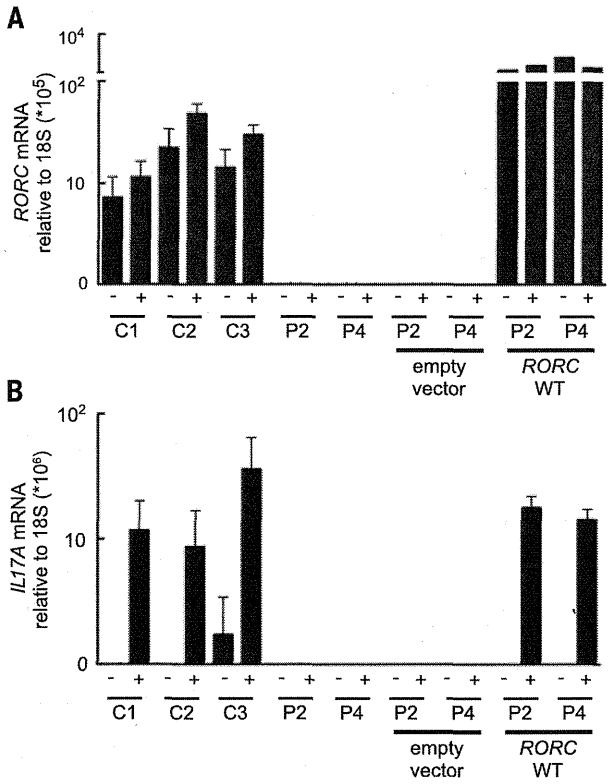

Fig. 4. T cell lines from *RORC*$^{-/-}$ patients fail to induce *IL17A* after mitogen stimulation. (**A**) *Herpesvirus saimiri*–transformed T cells from healthy donors (C1, C2, C3) or *RORC*$^{-/-}$ patients (P2, P4) were cultured in the presence (+) or absence (−) of PMA and ionomycin, and then total RNA was extracted and used for quantitative reverse transcription polymerase chain reaction for total *RORC*. T cell lines from *RORC*$^{-/-}$ patients were transduced with retrovirus encoding either a tag only (empty vector) or tagged WT *RORC* isoform 2. (**B**) *IL17A* expression was assessed in the same RNA samples presented in (A). *n* = 3 replicates; error bars represent SEM.

Conclusion

Collectively, these data demonstrate that human *RORC* plays a surprising dual role in host defense. These findings are clinically, immunologically, and genetically robust, as they were consistent in seven patients from three ethnic groups, homozygous for three different *RORC* mutations that are loss-of-function for both isoforms. Although the two infectious phenotypes are purely recessive, some immunological phenotypes showed codominant or dominant inheritance. The mild T cell lymphopenia, small thymus, lack of palpable axillary and cervical lymph nodes, and absence of MAIT and type 1 NKT cells in *RORC*$^{-/-}$ patients were consistent with the phenotype of *Rorc*$^{-/-}$ mice (table S3). Likewise, impaired IL-17A/F immunity was predicted to account for impaired protection against *Candida albicans* (*35*), as *Rorc* is the master gene controlling T$_H$17 differentiation in inbred mice (*11*), and mutations affecting human IL-17A/F immunity underlie isolated CMC (*1*, *26*, *36*). The IL-17A/F defect therefore underlies CMC in RORγT-deficient patients, probably but not necessarily because of T cells, as other cells can produce these cytokines in healthy individuals. We expected these patients to be susceptible to candidiasis, but their susceptibility to mycobacterial disease and its severity were unanticipated. This phenotype does not seem to be human-specific, as we also found that mice deficient for *Rorc* (*14*) are susceptible to mycobacterial infection (fig. S19). Our data conclusively demonstrate that human *RORC* plays an indispensable role in the induction of IFN-γ–dependent antimycobacterial systemic immunity. The mechanism underlying disease in these patients probably involves an impairment of the induction of IFN-γ production by γδ T cells, CCR6$^+$CXCR3$^+$CD4$^+$ αβ T$_H$1* cells, or both in response to mycobacteria. Other mechanisms may also be at work. Human *RORC* is essential not only for the development of IL-17A/F–producing lymphocytes protecting the mucocutaneous barriers against *Candida* but also for the activation of IFN-γ–producing T cells and for systemic protection against *Mycobacterium*.

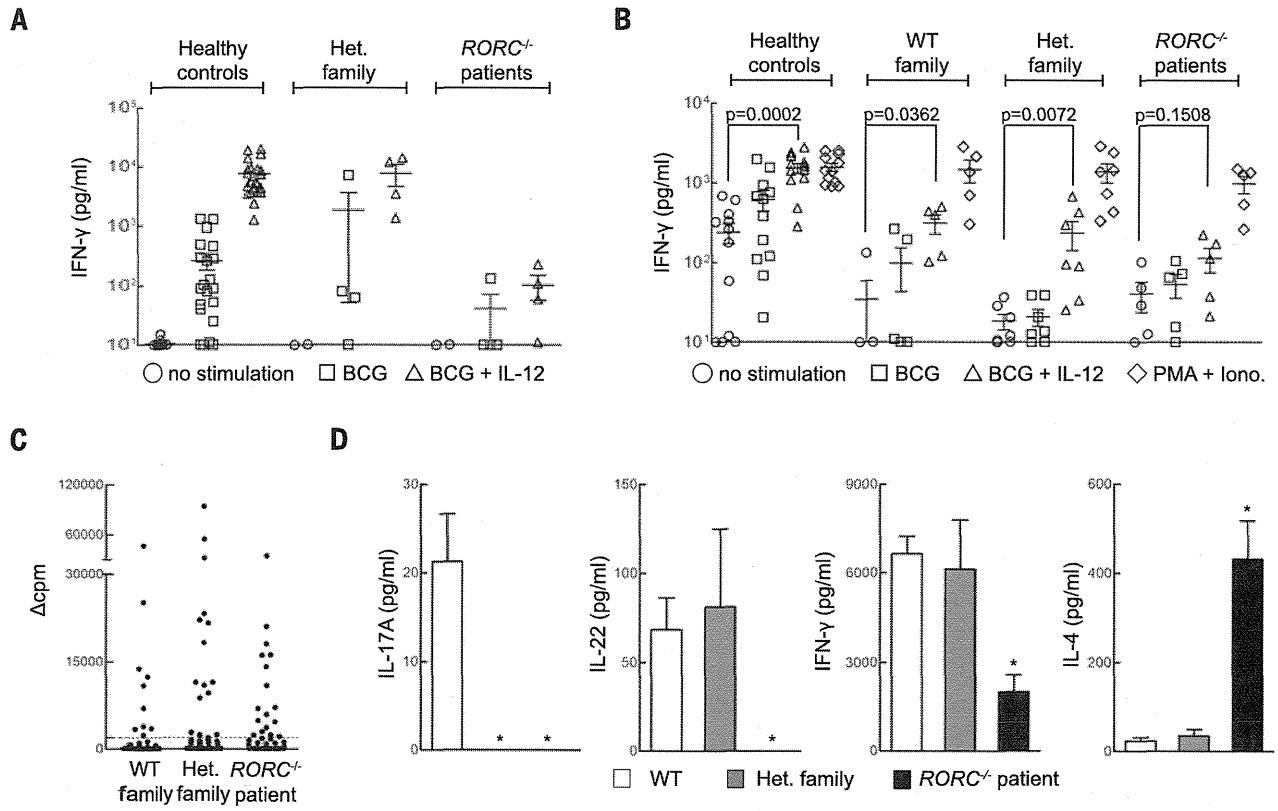

Fig. 5. Cellular mechanisms of impaired IFN-γ immunity to *Mycobacterium* in *RORC*$^{-/-}$ patients. (**A**) Whole-blood samples from healthy controls (n = 23), heterozygous family members (n = 4), or *RORC*$^{-/-}$ patients (n = 4) were incubated for 48 hours under three different sets of activation conditions: (i) medium alone, (ii) live *M. bovis*–BCG (BCG) at a multiplicity of infection of 20 BCG cells per leukocyte, and (iii) BCG plus 20 ng/ml IL-12. The IFN-γ levels of culture supernatants were determined by enzyme-linked immunosorbent assay (ELISA). (**B**) Equal numbers of live PBMCs from healthy controls, WT family members, heterozygous family members, or *RORC*$^{-/-}$ patients were cultured in the presence of live BCG, BCG and IL-12, or PMA/ionomycin for 48 hours. IFN-γ concentration in the culture supernatant was assessed by ELISA. (**C**) Sorted CCR6^{+} memory CD4^{+} T cells were polyclonally stimulated with PHA in the presence of irradiated allogeneic feeder cells and IL-2 to generate T cell libraries, as in Fig. 3D. Library screening was performed 14 to 21 days after initial stimulation by culturing thoroughly washed T cells with autologous irradiated B cells, with or without a 3-hour pulse with *M. bovis*–BCG peptide pools. Proliferation was measured by radiolabel incorporation on day 4 and is expressed as Δcpm values. Each symbol illustrates one culture. Dotted lines represent the cutoff value. The frequencies of specific T cells calculated using the Poisson distribution were 467/10^{6}, 749/10^{6}, and 875/10^{6} in WT control, heterozygous family member, and *RORC*$^{-/-}$ patient, respectively. (**D**) The cytokines indicated were determined in the culture supernatants from (C) for wells with Δcpm values above the cutoff value. Number of wells: n = 45 to 64 for WT controls, n = 4 to 10 for heterozygous family members, and n = 14 to 23 for *RORC*$^{-/-}$ patients. *P < 0.05 versus WT controls; in two-tailed Mann-Whitney tests with Bonferroni correction. Error bars in (D) indicate SEM.

REFERENCES AND NOTES

1. A. Puel *et al.*, *Science* **332**, 65–68 (2011).
2. Y. Ling *et al.*, *J. Exp. Med.* **212**, 619–631 (2015).
3. D. Bogunovic *et al.*, *Science* **337**, 1684–1688 (2012).
4. J. Bustamante, S. Boisson-Dupuis, L. Abel, J.-L. Casanova, *Semin. Immunol.* **26**, 454–470 (2014).
5. M. Kircher *et al.*, *Nat. Genet.* **46**, 310–315 (2014).
6. A. Medvedev, A. Chistokhina, T. Hirose, A. M. Jetten, *Genomics* **46**, 93–102 (1997).
7. I. Villey, R. de Chasseval, J. P. de Villartay, *Eur. J. Immunol.* **29**, 4072–4080 (1999).
8. Y. W. He, M. L. Deftos, E. W. Ojala, M. J. Bevan, *Immunity* **9**, 797–806 (1998).
9. Q. Ruan *et al.*, *J. Exp. Med.* **208**, 2321–2333 (2011).
10. G. Eberl, D. R. Littman, *Immunol. Rev.* **195**, 81–90 (2003).
11. I. I. Ivanov *et al.*, *Cell* **126**, 1121–1133 (2006).
12. J. Guo *et al.*, *Nat. Immunol.* **3**, 469–476 (2002).
13. X. O. Yang *et al.*, *Immunity* **28**, 29–39 (2008).
14. G. Eberl *et al.*, *Nat. Immunol.* **5**, 64–73 (2004).
15. C. E. Sutton *et al.*, *Immunity* **31**, 331–341 (2009).
16. M. L. Robinette *et al.*, *Nat. Immunol.* **16**, 306–317 (2015).
17. M. L. Michel *et al.*, *Proc. Natl. Acad. Sci. U.S.A.* **105**, 19845–19850 (2008).
18. T. Egawa *et al.*, *Immunity* **22**, 705–716 (2005).
19. D. F. Hoft, R. M. Brown, S. T. Roodman, *J. Immunol.* **161**, 1045–1054 (1998).
20. I. Van Rhijn *et al.*, *Nat. Immunol.* **14**, 706–713 (2013).
21. L. D. Notarangelo, *Annu. Rev. Immunol.* **31**, 195–225 (2013).
22. Z. Sun *et al.*, *Science* **288**, 2369–2373 (2000).
23. G. Eberl, D. R. Littman, *Science* **305**, 248–251 (2004).
24. H. Takatori *et al.*, *J. Exp. Med.* **206**, 35–41 (2009).
25. E. V. Acosta-Rodriguez *et al.*, *Nat. Immunol.* **8**, 639–646 (2007).
26. B. Boisson *et al.*, *Immunity* **39**, 676–686 (2013).
27. J. Feinberg *et al.*, *Eur. J. Immunol.* **34**, 3276–3284 (2004).
28. M. Ouederni *et al.*, *Blood* **118**, 5108–5118 (2011).
29. O. de la Calle-Martin *et al.*, *J. Clin. Invest.* **108**, 117–123 (2001).
30. B. Pasquier *et al.*, *J. Exp. Med.* **201**, 695–701 (2005).
31. E. Martin *et al.*, *Nature* **510**, 288–292 (2014).
32. A. C. Chan *et al.*, *Science* **264**, 1599–1601 (1994).
33. N. V. Morgan *et al.*, *J. Clin. Invest.* **121**, 695–702 (2011).
34. L. Le Bourhis *et al.*, *Nat. Immunol.* **11**, 701–708 (2010).
35. H. R. Conti *et al.*, *J. Exp. Med.* **206**, 299–311 (2009).
36. L. Liu *et al.*, *J. Exp. Med.* **208**, 1635–1648 (2011).
37. Materials and methods are available as supplementary materials on *Science* Online.

ACKNOWLEDGMENTS

We thank the patients and their families for their collaboration; both branches of the Laboratory of Human Genetics of Infectious Diseases for helpful discussions and support; M. Hindiyeh for expert clinical care of the patients from Kindred A; G. C. Tsokos for providing the *IL17A* reporter luciferase plasmid; E. Van de Vosse for providing the pLZRS-IRES-ΔNGFR vector; D. Littman for helpful discussions; B. Fleckenstein and M. Schmidt for the generation of patient-derived T cell lines; and Y. Nemirovskaya, L. Amar, E. Anderson, M. Courat, and T. Nivare for administrative support. The data presented in the manuscript are tabulated in the main paper and in the supplementary materials. The sequence data are available in the Sequence Read Archive (www.ncbi.nlm.nih.gov/sra) with accession numbers SRS964935, SRS965039, SRS965040, and SRS965042. J.Mc. and The University of Melbourne filed Australian provisional patent application numbers 2014901185 and 2014901 that relate to ligands that bind MR1 and stimulate MAIT cells. The Laboratory of Human Genetics of Infectious Diseases is supported by grants from the National Center for Research Resources and the National Center for Advancing Sciences,

NIH (8UL1TR000043); the French National Research Agency (ANR) under the "Investments for the Future" program (grant ANR-10-IAHU-01), grant IFNGPHOX (13-ISV3-0001-01 to J.B.), and grant GENCMCD (11-BSV3-005-01 to A.P); Laboratoire d'Excellence Integrative Biology of Emerging Infectious Diseases (ANR-10-LABX-62-IBEID); the National Health and Medical Research Council (NHMRC) (to E.K.D., C.S.M., S.G.T, and J.Mc.); the Rockefeller University; INSERM; Université Paris Descartes; the St. Giles Foundation; the National Institute of Allergy and Infectious Diseases (R37AI095983 to J.-L.C.); and the NIH (contract HHSN272200900044C to A.S.). S.O. was supported by Grants-in-Aid for Scientific Research from the Japan Society for the Promotion of Science (25713039 and 25670477), J.G.M. by the Canadian Institutes of Health Research, R.M.-B. by the European Molecular Biology Organization, Y.I. by the AXA Research Fund, L.A.H. by the Rheumatology Research Foundation's Scientist Development Award, and F.S. by grants from the European Research Council (323183 PREDICT) and the Swiss National Science Foundation (149475). The Institute for Research in Biomedicine and the Center of Medical Immunology are supported by the Helmut Horten Foundation. S.A.-M. is the bronchial asthma research chair of the Prince Naif Center for Immunology Research.

SUPPLEMENTARY MATERIALS

www.sciencemag.org/content/349/6248/606/suppl/DC1
Materials and Methods
Supplementary Text
Figs. S1 to S19
Tables S1 to S3
References (*38–67*)

7 December 2014; accepted 29 June 2015
Published online 9 July 2015
10.1126/science.aaa4282

TOPOLOGICAL MATTER

Discovery of a Weyl fermion semimetal and topological Fermi arcs

Su-Yang Xu,[1,2*] Ilya Belopolski,[1*] Nasser Alidoust,[1,2*] Madhab Neupane,[1,3*] Guang Bian,[1] Chenglong Zhang,[4] Raman Sankar,[5] Guoqing Chang,[6,7] Zhujun Yuan,[4] Chi-Cheng Lee,[6,7] Shin-Ming Huang,[6,7] Hao Zheng,[1] Jie Ma,[8] Daniel S. Sanchez,[1] BaoKai Wang,[6,7,9] Arun Bansil,[9] Fangcheng Chou,[5] Pavel P. Shibayev,[1,10] Hsin Lin,[6,7] Shuang Jia,[4,11] M. Zahid Hasan[1,2†]

A Weyl semimetal is a new state of matter that hosts Weyl fermions as emergent quasiparticles and admits a topological classification that protects Fermi arc surface states on the boundary of a bulk sample. This unusual electronic structure has deep analogies with particle physics and leads to unique topological properties. We report the experimental discovery of a Weyl semimetal, tantalum arsenide (TaAs). Using photoemission spectroscopy, we directly observe Fermi arcs on the surface, as well as the Weyl fermion cones and Weyl nodes in the bulk of TaAs single crystals. We find that Fermi arcs terminate on the Weyl fermion nodes, consistent with their topological character. Our work opens the field for the experimental study of Weyl fermions in physics and materials science.

Weyl fermions have long been known in quantum field theory, but have not been observed as a fundamental particle in nature (*1–3*). Recently, it was understood that a Weyl fermion can emerge as a quasiparticle in certain crystals, Weyl fermion semimetals (*1–22*). Despite being a gapless metal, a Weyl semimetal is characterized by topological invariants, broadening the classification of topological phases of matter beyond insulators. Specifically, Weyl fermions at zero energy correspond to points of bulk band degeneracy, Weyl nodes, which are associated with a chiral charge that protects gapless surface states on the boundary of a bulk sample. These surface states take the form of Fermi arcs connecting the projection of bulk Weyl nodes in the surface Brillouin zone (BZ) (*6*). A band structure like the Fermi arc surface states would violate basic band theory in an isolated two-dimensional (2D) system and can only arise on the boundary of a 3D sample, providing a dramatic example of the bulk-boundary correspondence in a topological phase. In contrast to topological insulators where only the surface states are interesting (*21, 22*), a Weyl semimetal features unusual band structure in the bulk and on the surface. The Weyl fermions in the bulk are predicted to provide a condensed-matter realization of the chiral anomaly, giving rise to a negative magnetoresistance under parallel electric and magnetic fields, unusual optical conductivity, nonlocal transport, and local non-conservation of ordinary current (*5, 12–16*). At the same time, the Fermi arc surface states are predicted to show unconventional quantum oscillations in magneto-transport, as well as unusual quantum interference effects in tunneling spectroscopy (*17–19*). The prospect of the realization of these phenomena has inspired much experimental and theoretical work (*1–22*).

Here we report the experimental realization of a Weyl semimetal in a single crystalline material, tantalum arsenide (TaAs). Using the combination of the vacuum ultraviolet (low-photon-energy) and soft x-ray (SX) angle-resolved photoemission spectroscopy (ARPES), we systematically and differentially study the surface and bulk electronic structure of TaAs. Our ultraviolet (low-photon-energy) ARPES measurements, which are highly surface sensitive, demonstrate the existence of the Fermi arc surface states, consistent with our band calculations presented here. Moreover, our SX-ARPES measurements, which are reasonably bulk sensitive, reveal the 3D linearly dispersive bulk Weyl cones and Weyl nodes. Furthermore, by combining the low-photon-energy and SX-ARPES data, we show that the locations of the projected bulk Weyl nodes correspond to the terminations of the Fermi arcs within our experimental resolution. These systematic measurements demonstrate TaAs as a Weyl semimetal.

The material system and theoretical considerations

Tantalum arsenide is a semimetallic material that crystallizes in a body-centered tetragonal lattice system (Fig. 1A) (*23*). The lattice constants are a = 3.437 Å and c = 11.656 Å, and the space group is $I4_1md$ (#109, C_{4v}), as consistently reported in previous structural studies (*23–25*). The crystal consists of interpenetrating Ta and As sublattices, where the two sublattices are shifted by $(\frac{a}{2}, \frac{a}{2}, \delta)$, $\delta \approx \frac{c}{12}$. Our diffraction data match well with the lattice parameters and the space group $I4_1md$ (*26*). The scanning tunneling microscopic (STM) topography (Fig. 1B) clearly resolves the (001) square lattice without any obvious defect. From the topography, we obtain a lattice constant a = 3.45 Å. Electrical transport measurements on TaAs confirmed its semimetallic transport properties and reported negative magnetoresistance, suggesting the anomalies due to Weyl fermions (*23*).

We discuss the essential aspects of the theoretically calculated bulk band structure (*9, 10*) that predicts TaAs as a Weyl semimetal candidate. Without spin-orbit coupling, calculations (*9, 10*) show that the conduction and valence bands interpenetrate (dip into) each other to form four 1D line nodes (closed loops) located on the k_x and k_y planes (shaded blue in Fig. 1, C and E). Upon the inclusion of spin-orbit coupling, each line node loop is gapped out and shrinks into six Weyl nodes that are away from the $k_x = 0$ and $k_y = 0$ mirror planes (Fig. 1E, small filled circles). In our calculation, in total there are 24 bulk Weyl cones (*9, 10*), all of which are linearly dispersive and are associated

[1]Laboratory for Topological Quantum Matter and Spectroscopy (B7), Department of Physics, Princeton University, Princeton, NJ 08544, USA. [2]Princeton Center for Complex Materials, Princeton Institute for Science and Technology of Materials, Princeton University, Princeton, NJ 08544, USA. [3]Condensed Matter and Magnet Science Group, Los Alamos National Laboratory, Los Alamos, NM 87545, USA. [4]International Center for Quantum Materials, School of Physics, Peking University, China. [5]Center for Condensed Matter Sciences, National Taiwan University, Taipei 10617, Taiwan. [6]Centre for Advanced 2D Materials and Graphene Research Centre National University of Singapore, 6 Science Drive 2, Singapore 117546. [7]Department of Physics, National University of Singapore, 2 Science Drive 3, Singapore 117542. [8]Quantum Condensed Matter Division, Oak Ridge National Laboratory, Oak Ridge, TN 37831, USA. [9]Department of Physics, Northeastern University, Boston, MA 02115, USA. [10]Princeton Institute for Science and Technology of Materials, Princeton University, Princeton, NJ 08544, USA. [11]Collaborative Innovation Center of Quantum Matter, Beijing, 100871, China.
*These authors contributed equally to this work. †Corresponding author. E-mail: mzhasan@princeton.edu

A Novel In-Frame Deletion in the Leucine Zipper Domain of C/EBP ε Leads to Neutrophil-Specific Granule Deficiency

Taizo Wada, Tadayuki Akagi, Masahiro Muraoka, Tomoko Toma, Kenzo Kaji, Kazunaga Agematsu, H. Phillip Koeffler, Takashi Yokota and Akihiro Yachie

J Immunol 2015; 195:80-86; Prepublished online 27 May 2015;
doi: 10.4049/jimmunol.1402222
http://www.jimmunol.org/content/195/1/80

The Journal of Immunology is published twice each month by The American Association of Immunologists, Inc., 9650 Rockville Pike, Bethesda, MD 20814-3994.

Print ISSN: 0022-1767 Online ISSN: 1550-6606.

A Novel In-Frame Deletion in the Leucine Zipper Domain of C/EBPε Leads to Neutrophil-Specific Granule Deficiency

Taizo Wada,*[,1] Tadayuki Akagi,[†,1] Masahiro Muraoka,* Tomoko Toma,* Kenzo Kaji,[‡] Kazunaga Agematsu,[§] H. Phillip Koeffler,[¶,‖] Takashi Yokota,[†] and Akihiro Yachie*

Neutrophil-specific granule deficiency (SGD) is a rare autosomal recessive primary immunodeficiency characterized by neutrophil dysfunction, bilobed neutrophil nuclei and lack of neutrophil-specific granules. Defects in a myeloid-specific transcription factor, CCAAT/enhancer binding protein-ε (C/EBPε), have been identified in two cases in which homozygous frameshift mutations led to loss of the leucine zipper domain. In this study, we report a 55-y-old woman affected with SGD caused by a novel homozygous 2-aa deletion (ΔRS) in the leucine zipper domain of the C/EBPε gene. The patient showed characteristic neutrophil abnormalities and recurrent skin infections; however, there was no history of deep organ infections. Biochemical analysis revealed that, in contrast to the two frameshift mutations, the ΔRS mutant maintained normal cellular localization, DNA-binding activity, and dimerization, and all three mutants exhibited marked reduction in transcriptional activity. The ΔRS mutant was defective in its association with Gata1 and PU.1, as well as aberrant cooperative transcriptional activation of eosinophil major basic protein. Thus, the ΔRS likely impairs protein-protein interaction with other transcription factors, resulting in a loss of transcriptional activation. These results further support the importance of the leucine zipper domain of C/EBPε for its essential function, and indicate that multiple molecular mechanisms lead to SGD. *The Journal of Immunology*, **2015, 195: 80–86.**

Neutrophil-specific granule deficiency (SGD) is a rare autosomal recessive primary immunodeficiency characterized by either profound reduction or absence of neutrophil-specific granules and bilobed neutrophil nuclei (pseudo–Pelgar-Huët anomaly) (1). It was previously called "lactoferrin deficiency." Patients with SGD exhibit increased susceptibility to bacterial infections, especially affecting the skin, ears, lungs, and lymph nodes. The gene responsible for SGD is the CCAAT/enhancer binding protein-ε (C/EBPε) gene. To date, two patients have been reported who carry C/EBPε frameshift mutations that result in abrogated protein expression (2, 3). In addition, another patient with SGD had a heterozygous missense mutation of the C/EBPε gene, but this mutation was unlikely to have caused disease because it resulted in elevated levels of C/EBPε (4). In this patient, the growth factor independence 1 (Gfi-1) protein that represses transcription of C/EBPε was decreased, although the patient had no mutation of the Gfi-1 gene. Taken together, these previous findings suggest that SGD is a genetically heterogeneous disease. Because of the extreme rarity of SGD, the full spectrum of clinical symptoms and cellular abnormalities of the disease is unclear.

C/EBPε is a member of the C/EBP family of widely expressed transcription factors that regulate proliferation, differentiation, and apoptosis in a variety of cell types (5, 6). The C/EBP family consists of six members (C/EBPα, β, γ, δ, ε, and ζ), and cellular expression of each C/EBP is tightly regulated. They bind to DNA through the highly conserved basic leucine zipper (bZIP) domain. C/EBPε is restricted to granulocytes and is essential for their terminal differentiation (6, 7). C/EBPε transcription primarily occurs at the myelocyte–metamyelocyte stage of differentiation and decreases in polymorphonuclear neutrophils. The human C/EBPε gene produces four isoforms of 32, 30, 27, and 14 kDa that are functionally different; only the 32-kDa C/EBPε has full transactivating potential (8–10). C/EBPε is indispensable for expression of genes encoding proteins that reside in specific granules of neutrophils, such as lactoferrin and defensins. Many features of SGD are manifested by C/EBPε-deficient mice in which neutrophils are morphologically and functionally abnormal and eosinophil numbers are decreased (8).

In this study, we describe another case of SGD with a novel 2-aa deletion in the bZIP domain of C/EBPε, and we report the mechanism that leads to SGD. We also completed clinical, cellular, and molecular comparisons for this patient and the previously reported two cases of SGD (2, 3), and we discuss the functional significance of the mutation.

Materials and Methods

Patients

We studied two Japanese patients with SGD. Patient P1 is a 55-y-old woman who has suffered since late infancy from recurrent skin infections that often required more than 2 mo to heal. After hospitalization because of severe

*Department of Pediatrics, Institute of Medical, Pharmaceutical and Health Sciences, School of Medicine, Kanazawa University, Kanazawa 920-8641, Japan; [†]Department of Stem Cell Biology, Institute of Medical, Pharmaceutical and Health Sciences, School of Medicine, Kanazawa University, Kanazawa 920-8640, Japan; [‡]Department of Dermatology, Komatsu Municipal Hospital, Komatsu 923-0961, Japan; [§]Department of Infection and Host Defense, Shinshu University Graduate School of Medicine, Matsumoto 390-8621, Japan; [¶]Division of Hematology and Oncology, Cedars-Sinai Medical Center, University of California Los Angeles School of Medicine, Los Angeles, CA 90048; and [‖]Cancer Science Institute of Singapore, National University of Singapore, Singapore 117599, Singapore

[1]T.W. and T.A. contributed equally to this work.

Received for publication September 8, 2014. Accepted for publication May 4, 2015.

This work was supported by a Grant-in-Aid for Scientific Research from the Ministry of Education, Culture, Sports, Science and Technology of Japan and a grant from the Ministry of Health, Labor, and Welfare of Japan, Tokyo.

Address correspondence to Dr Taizo Wada, Department of Pediatrics, School of Medicine, Institute of Medical, Pharmaceutical and Health Sciences, Kanazawa University, 13-1 Takaramachi, Kanazawa 920-8641, Japan. E-mail address: taizo@staff.kanazawa-u.ac.jp

The online version of this article contains supplemental material.

Abbreviations used in this article: bZIP, basic leucine zipper; C/EBPε, CCAAT/enhancer binding protein-ε; Gata1, GATA binding protein 1; MaBP, major basic protein; MBP, maltose-binding protein; NGAL, neutrophil gelatinase-associated lipocalin; Prg2, proteoglycan 2; SGD, neutrophil-specific granule deficiency; WT, wild-type.

www.jimmunol.org/cgi/doi/10.4049/jimmunol.1402222

otitis media at 54 y of age, she was referred to our hospital for suspected immunodeficiency. A history of parental consanguinity appeared likely. However, her father had already died of a heart attack, and her mother refused genetic analysis. Her elder brother had similar skin symptoms and died of enterocolitis at 10 y of age. Another brother also died early after birth from unspecified causes. Two children of patient P1 and her granddaughter were healthy, and they did not want genetic testing. Clinical and genetic data of patient P2 have already been published (3, 11). Patient P2 is now 40 y old. Approval for the study was obtained from the Human Research Committee of Kanazawa University Graduate School of Medical Science, and informed consent was provided according to the Declaration of Helsinki.

Flow cytometry and immunohistochemistry

For flow cytometric analysis, the following mAbs were used: FITC-conjugated anti-CD16, anti-CD32 or CD66b and PE-conjugated anti-CD11b, anti-CD14, anti-CD15 anti-CD16 or anti-CD64 (BD, San Diego, CA); and FITC-conjugated anti-CD16b and PE-conjugated CD11c (Beckman Coulter, Fullerton, CA). Analysis was performed on a FACSCalibur using CellQuest software (BD Biosciences, Tokyo, Japan) (12). Cytospin preparations were made using whole leukocytes. For lactoferrin staining, cytospin samples were stained with anti-lactoferrin mAb (Beckman Coulter), followed by universal immuno-alkaline-phosphatase polymer (Simple Stain AP; Nichirei Biosciences, Tokyo, Japan). The alkaline phosphatase activity was visualized using Fast Red TR salt and Naphtol AS-MX phosphate (Sigma-Aldrich, St. Louis, MO). For analysis of internal alkaline phosphatase and peroxidase activity, alkaline phosphatase substrate solution (BCIP/NBT Substrate System; DAKO, Glostrup, Denmark) and a peroxidase staining kit (Muto Pure Chemicals, Tokyo, Japan) were used, respectively.

Mutation analysis

Peripheral blood or buccal mucosa samples, or both, were obtained from patients, and DNA was extracted from the samples using a standard method. Direct sequencing of the C/EBPε gene was performed as described previously (2).

Cell culture and RT-PCR

Human embryonic kidney (HEK) 293 and mouse NIH3T3 cells were cultured in DMEM containing either 10% FBS or 10% calf serum, respectively. Total RNA was extracted from transfected NIH3T3 cells with Sepasol-RNA I Super G (Nacalai Tesque, Kyoto, Japan) and converted to cDNAs by ReverTraAce (Toyobo, Tokyo, Japan). Expression of human C/EBPε and PU.1, and murine cathelicidin B9/neutrophil granule protein, neutrophil gelatinase-associated lipocalin (NGAL)/ lipocalin 2, lactoferrin, proteoglycan 2 (Prg2)/eosinophil granule eosinophil major basic protein (MaBP), GATA binding protein 1 (Gata1), and GAPDH was examined by RT-PCR. Primer sequences are reported in Supplemental Table I. The number of amplification cycles was 20 for GAPDH; 25 for C/EBPε, PU.1, MaBP, and Gata1; 30 for B9 and NGAL; and 35 for lactoferrin. The PCR cycle consisted of 94°C for 15 s, 60°C for 30 s, and 72°C for 30 s. For lactoferrin, the annealing temperature was 64°C. All PCR reactions were completed with Taq polymerase (Ampliqon, Odense, Denmark) except for C/EBPε (PrimeSTAR Max DNA Polymerase; Takara Bio, Otsu, Japan).

Construction of plasmid, luciferase assay, and cellular localization

Construction of mammalian expression vectors, including pCMV5-Flag maltose-binding protein (MBP), pCAGIP-enhanced GFP, and pCAGIP-Myc, was described previously (13, 14). Coding region of wild-type (WT) human C/EBPε and its mutants, ΔRS, del5bp, and insA, were amplified by PCR using specific primers (Supplemental Table I) and cloned into expression vectors. Murine Gata1 and human PU.1 expression vectors were described previously (15), and their coding regions were cloned into the pCAGIP-Myc vector. The luciferase reporter plasmid containing the G-CSF receptor promoter (pGCSFR-Luc) has been described previously (16). The reporter plasmid, C/EBPε and C/EBPε mutant expression vectors (ΔRS, del5bp, and insA), were transfected into HEK293 cells by Lipofectamine 2000 (Life Technologies, Grand Island, NY). To determine luciferase activity, cell extracts were prepared 48 h after transfection, and luciferase activity was measured with a luciferase assay kit (Promega, Madison, WI) using an AB-2200 luminometer (ATTO, Tokyo, Japan). Protein concentration of each sample was measured by Protein Assay CBB solution (Nacalai Tesque). Amounts of cell extracts used to obtain relative luciferase activities were normalized to 1 μg total protein per sample. To observe cellular localization of C/EBPε and its mutants, GFP-tagged fusion protein expression vectors were introduced into NIH3T3 cells. Nuclei were stained by Hoechst 33258 (Sigma). Signals were observed 48 h after transfection.

Biotin-labeled DNA pull-down assay, MBP pull-down assay, and Western blot analysis

Biotin-labeled DNA pull-down assay was performed as described previously (13, 17). Briefly, biotin-labeled oligonucleotides containing the human lactoferrin gene C/EBPε binding site (5′-GGGTGTCTATTGGGCAACAGGGCGGG-3′) were incubated with cell extracts from HEK293 cells transfected with either pCAGIP-Myc-C/EBPε or its mutant counterparts (ΔRS, del5bp, and insA) in the presence of streptavidin-agarose (Novagen, Darmstadt, Germany). Twenty-five-fold nonlabeled oligonucleotides (either WT or mutant nonbinding control) were added for the competition assays. The beads were washed three times with a washing buffer, and the bound proteins were eluted by boiling in 2X SDS sample buffer. Samples were then examined by Western blot analysis as described below. MBP pull-down assay was performed as described previously (13, 17). HEK293 cells were cotransfected with pCAGIP-Myc-C/EBPε (WT or ΔRS) and pCMV5-Flag-MBP-C/EBPε (WT or ΔRS). HEK293 cells were also cotransfected with pCAGIP-Myc-Gata1 and pCMV5-Flag-MBP-C/EBPε or its mutant counterparts, or with pCAGIP-Myc-PU.1 and pCMV5-Flag-MBP-C/EBPε or its mutant counterparts. MBP-fused proteins were pulled down by amylose resin, and the precipitates were analyzed by Western blot analysis. For Western blot analysis, samples were subjected to SDS-PAGE and transferred to a nitrocellulose membrane. The membrane was incubated with either anti-Myc (sc-40; Santa Cruz Biotechnology, Santa Cruz, CA) or anti-Flag (F3165; Sigma-Aldrich) Abs followed by HRP-conjugated anti-mouse Ab (Millipore, Billerica, MA). The blot was visualized using ECL reagents (PerkinElmer, Waltham, MA) with an LAS-1000 image analyzer (Fuji Film, Tokyo, Japan).

Results

Bilobed nucleus and lack of granules in neutrophils

Patient P1 exhibited an ulcerative skin abscess and numerous skin scars (Fig. 1A, 1B). Her peripheral blood smear showed unique bilobed nuclei and a lack of cytoplasmic granules in her neutrophils (Fig. 1C). Absence of eosinophils, increased basophils with normal cytoplasmic granularity, and monocytosis were also noted on smears of the peripheral blood (data not shown). The immunohistochemical analysis of her neutrophils clearly demonstrated the presence of peroxidase, a primary granule protein, and the absence

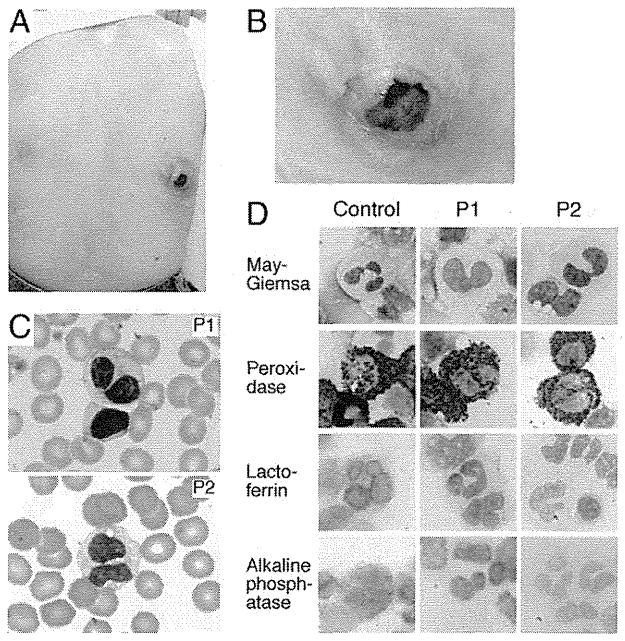

FIGURE 1. Patient characteristics. (**A** and **B**) Skin abscess with ulceration and scar. (**C**) Peripheral blood smears. Neutrophils from patients P1 and P2 have bilobed nuclei and lack cytoplasmic granules (May–Grünewald–Giemsa staining). Original magnification ×400. (**D**) Immunohistochemial analysis. Cytospin preparations of leukocytes stained with anti-lactoferrin mAb. Cellular alkaline phosphatase and peroxidase activity were also analyzed. Original magnification ×400.

of lactoferrin and alkaline phosphatase, both of which are normally expressed in specific granules of normal neutrophils (Fig. 1D). These characteristic features were similar to those of patient P2, the second case of genetically defined SGD, who carries a homozygous C/EBPε mutation, c.508_509insA (insA) (3).

Flow cytometric analysis of peripheral blood showed lower side scatter of P1 neutrophils compared with normal controls (Fig. 2) (18). More importantly, the majority of the patient's neutrophils that were defined on the basis of forward and side scatter expressed a monocyte marker CD14, indicating aberrant development toward the monocyte pathway. These cells did not express neutrophil markers such as CD15, CD16b (FcγRIIIB), and CD66b. Although CD64 (FcγRI) was not detected on her neutrophils and monocytes, CD11b, CD11c, and CD32 (FcγRII) were detectable equally on both cells (data not shown). Again, all these characteristic features were similar to those of patient P2. Neutrophils from patient P2 showed more CD16 expression compared with P1.

2-aa deletion in bZIP and reduced transcriptional activity

Direct sequence analysis revealed that patient P1 had a homozygous 6-bp deletion in exon 2 of the C/EBPε gene (c.739_744delCGCAGC). This novel mutation leads to a 2-aa deletion, p.Arg247_Ser248del (ΔRS), which is located in the bZIP domain (Fig. 3). The mutation was present in DNA isolated from both the peripheral blood and buccal mucosa, indicating a germline mutation, not a somatic one. Analysis of 100 alleles of ethnically matched healthy controls demonstrated the absence of the mutation in the general population.

To evaluate the transcriptional activation by the ΔRS mutant, HEK293 cells were cotransfected with a G-CSF receptor promoter reporter construct and C/EBPε expression vectors. As shown in Fig. 4A, WT C/EBPε presented robust reporter activity, whereas the ΔRS mutant exhibited a significant decrease in activity, similar to the previously reported mutants, insA and del5bp (c.249_253delTGACC) (2, 3), both of which were frameshift mutations with truncated proteins. HEK 293 cells transfected with the ΔRS mutant expressed levels of C/EBPε comparable to wild-type, as assessed with Western blot analysis, indicating ΔRS does not cause instability in the mutated C/EBPε protein (Fig. 4B). Increasing amounts of ΔRS had no negative effect on reporter activity of WT C/EBPε, indicating a lack of a dominant-negative effect of ΔRS on transcriptional activity (Fig. 4C). We also analyzed the ability of the C/EBPε mutant proteins to activate gene expression of secondary granule genes. As shown in Fig. 4D, WT C/EBPε was able to induce expression of endogenous B9, NGAL, and lactoferrin genes in transiently transfected NIH3T3 cells. In contrast, none of these genes was amplified from cells transfected with either the ΔRS mutant or the insA and del5bp mutants, consistent with loss of their capability to activate secondary granule genes.

Unaltered cellular localization, DNA-binding, and dimerization

To understand the mechanism by which the ΔRS mutation decreases transcriptional activity, we first investigated the cellular localization of WT and mutant C/EBPε proteins. GFP fluorescence was diffusely detected within the cytoplasm of NIH3T3 cells transfected with the control GFP vector, whereas WT and ΔRS mutant C/EBPε tagged with GFP was found in the nucleus (Fig. 5). Consistent with

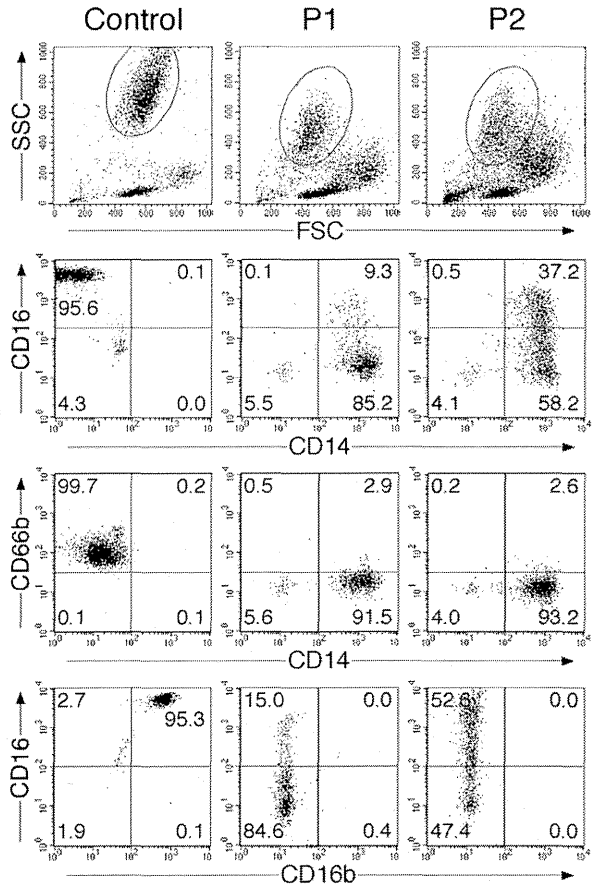

FIGURE 2. Characterization of granulocytes. Granulocytes were gated for fluorescence analysis. The percentage of cells gated in each region is shown.

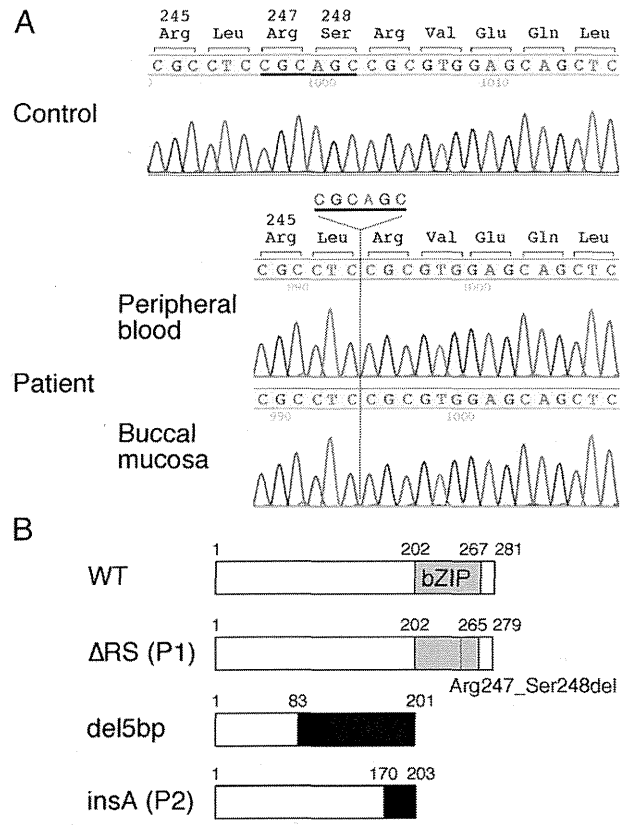

FIGURE 3. Mutation analysis of C/EBPε gene. (**A**) C/EBPε gene exon 2 was amplified from DNA extracted from normal control, as well as peripheral blood and buccal mucosa of patient P1. Direct sequencing was performed using an automated sequencer. A thick bar highlights the position of the 6-bp deletion (ΔRS). (**B**) Predicted structures of mutated C/EBPε molecules. The previously reported frameshift mutations, del5bp and insA, produced frameshifts that result in incorrect amino acid sequence subsequent to the mutations (shaded area) and premature termination.

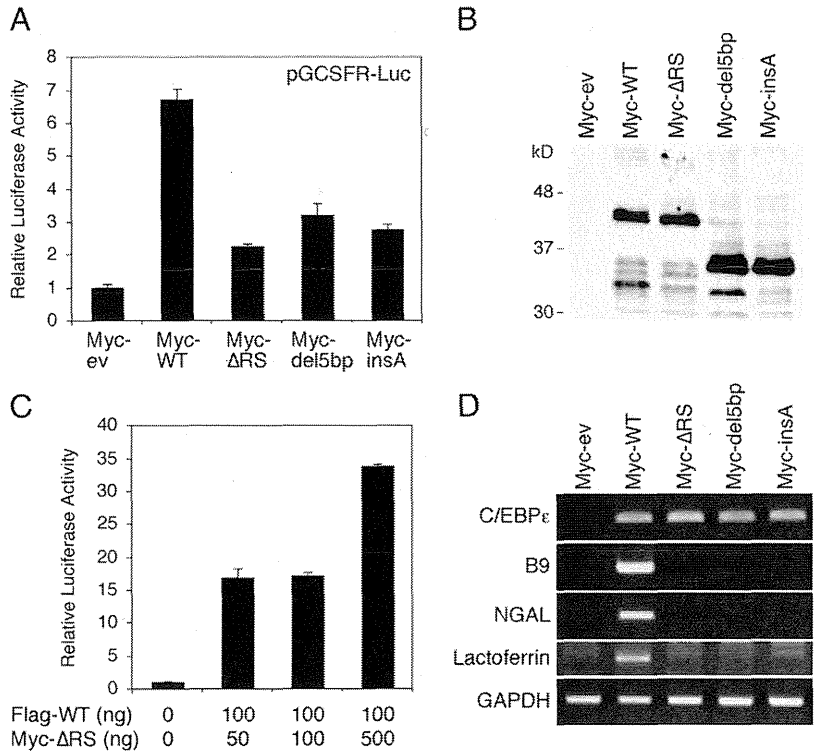

FIGURE 4. Transcriptional activity and induction of endogenous expression of granule genes. (**A**) Luciferase reporter plasmid containing the G-CSF receptor promoter (pGCSFR-Luc) was transfected into HEK293 cells with either control empty (ev), WT, ΔRS, del5bp, or insA C/EBPε expression vector. Luciferase activity was measured 48 h after transfection. Bars represent the means and SDs of triplicate assay. (**B**) Western blot analysis of C/EBPε was performed using lysates of HEK293 cells transfected with ev, WT, ΔRS, del5bp or insA C/EBPε vector. (**C**) WT C/EBPε vector was mixed with increasing amounts of ΔRS C/EBPε vector, and luciferase reporter assay was performed. (**D**) Expression vectors of ev, WT, ΔRS, del5bp, or insA C/EBPε were transfected into NIH3T3 cells, and expression of endogenous B9, NGAL, and lactoferrin was examined by RT-PCR. GAPDH was used as a loading control. The numbers of PCR cycles were 20 for GAPDH; 30 for C/EBPε, B9, and NGAL; and 35 for lactoferrin.

the previous report (3), the insA mutant was localized in the cytoplasm and the nucleus; and a similar abnormal localization was detected in the del5bp.

We next assessed the ability of the WT and mutant C/EBPε to bind to C/EBPε binding site at the 5′UTR of human lactoferrin gene (19). The oligonucleotides containing the C/EBPε binding site bound in vitro to C/EBPε from lysates of HEK293 cells transfected with WT Myc-C/EBPε vector (Fig. 6A, *top left blot*). Importantly, the ΔRS mutant showed DNA-binding ability comparable to the WT C/EBPε (Fig. 6A, *top right blot*). Nonlabeled oligonucleotides of the same sequence, but not those with a mutated sequence, were able to compete with the biotinylated oligonucleotides for sequence-specific binding of both the WT and ΔRS mutant C/EBPε. In contrast, no product was precipitated from lysates of cells transfected with the del5bp and the insA mutants, indicating that no oligonucleotide binding took place (Fig. 6A, *bottom panels*).

To assess further the functionality of the ΔRS mutant, we examined dimer formation in lysates of HEK293 cells cotransfected with Myc-C/EBPε and Flag-MBP-C/EBPε vectors. The ΔRS mutant was able to homodimerize or heterodimerize with WT C/EBPε at levels comparable to WT C/EBPε (Fig. 6B and data not shown). These results were consistent with the ability of the ΔRS mutant to bind to DNA.

Aberrant association with Gata1 and PU.1

To determine whether the ΔRS mutant properly interacts with other proteins, cooperative transcriptional activation of MaBP was analyzed in NIH3T3 cells. Consistent with the previous report (15), MaBP gene expression was observed in cells transfected with Gata1 and PU.1 in addition to WT C/EBPε, and no products were obtained from those without WT C/EBPε (Fig. 7A). Interestingly, the ΔRS mutant, as well as the del5bp and the insA mutants, failed to induce MaBP gene expression.

To assess further the ability of the C/EBPε mutants to bind to Gata1 as well as PU.1, the MBP pull-down assay was performed. As expected, both Gata1 and PU.1 were able to bind in vitro to C/EBPε in lysates of HEK293 cells transfected with the WT Flag-MBP-C/EBPε vector, and no binding was observed in lysates of cells transfected with the del5bp and the insA mutants (Fig. 7B, 7C). Some binding of the ΔRS mutant to Gata1 or PU.1 was indicated by the results, but the amounts of precipitated Gata1 and PU.1 were extremely low in lysates from HEK293 cells transfected with the ΔRS mutant.

Discussion

C/EBPε is essential for terminal differentiation of granulocytes. Frameshift mutations of the C/EBPε gene have been identified in two patients with SGD. In this study, we report on a 55-y-old woman (P1) affected with SGD caused by a novel 2-aa deletion mutation of the C/EBPε gene. This case represents a third case of genetically defined SGD. The availability of blood samples from the previous case (P2) offered us the unique opportunity to evaluate and compare phenotype of peripheral neutrophils in these patients. In addition to the morphologic abnormalities typical for SGD, we found characteristic surface phenotype in their neutrophils,

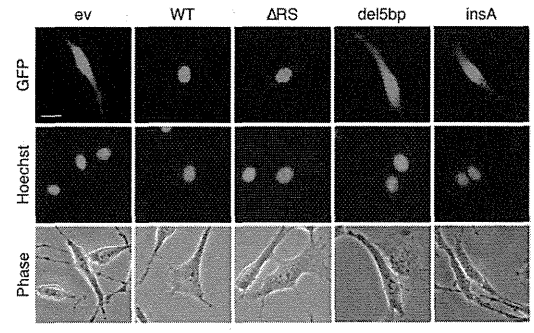

FIGURE 5. Cellular localization. GFP-tagged to either control empty (ev), WT (WT), ΔRS, del5bp or insA C/EBPε expression vectors were transfected into NIH3T3 cells, and cells were analyzed by microscopy and fluorescent microscopy 2 d after transfection. Nuclei were stained with Hoechst stain. Scale bar, 20 μm.

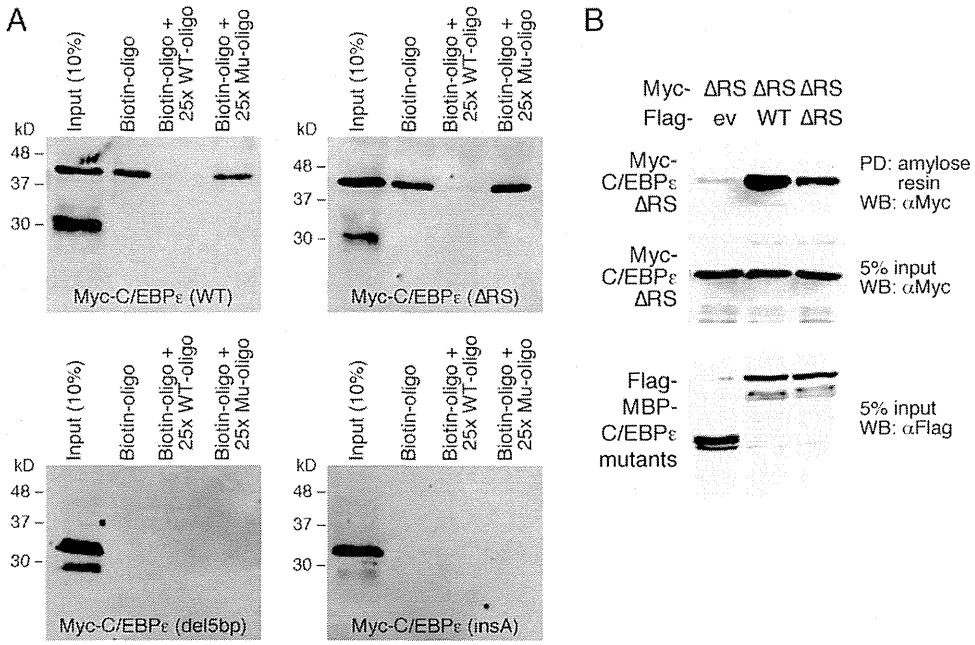

FIGURE 6. DNA binding activity and dimerization. (**A**) DNA binding activity of WT, ΔRS, del5bp, and insA C/EBPε. Biotin-labeled oligonucleotide containing the C/EBPε-binding site of the lactoferrin gene was incubated with Myc-C/EBPε (WT, ΔRS, del5bp, or insA)-transfected HEK293 cell extracts either with or without 25-fold nonlabeled WT or mutated nonbinding (μ) oligonucleotide. Biotin-labeled oligonucleotides were pulled down by streptavidin-agarose. The precipitates and cell lysates were analyzed by Western blot analysis with anti-Myc Ab. (**B**) Dimer formation of ΔRS. HEK293 cells were transfected with Myc-C/EBPε-ΔRS together with either empty control vector (MBP-ev), Flag-MBP-C/EBPε-WT or -ΔRS. MBP-fused proteins were pulled down by amylose resin, and the precipitates were analyzed by Western blot analysis with anti-Myc Ab. Expression of each protein was confirmed with anti-Myc and anti-Flag Abs, respectively.

including the presence of monocyte markers such as CD14 and the absence of neutrophil markers such as CD15, CD16b, and CD66b. It is therefore difficult to distinguish neutrophils from monocytes by surface markers in the patients. CD16 includes two isoforms, CD16a (FcγRIIIA) and CD16b. CD16a is a transmembrane receptor expressed by monocytes, natural killer cells and natural killer T cells, whereas CD16b is a GPI-anchored receptor that is thought to be expressed exclusively by neutrophils. Because pan-CD16 but not CD16b was detected in a subset of the patient's neutrophils, they likely expressed CD16a. Neutrophils from patient P2 showed higher levels of CD16 expression than those of patient P1 did, indicating a larger subpopulation of $CD16a^{+}$ neutrophils. Human monocytes

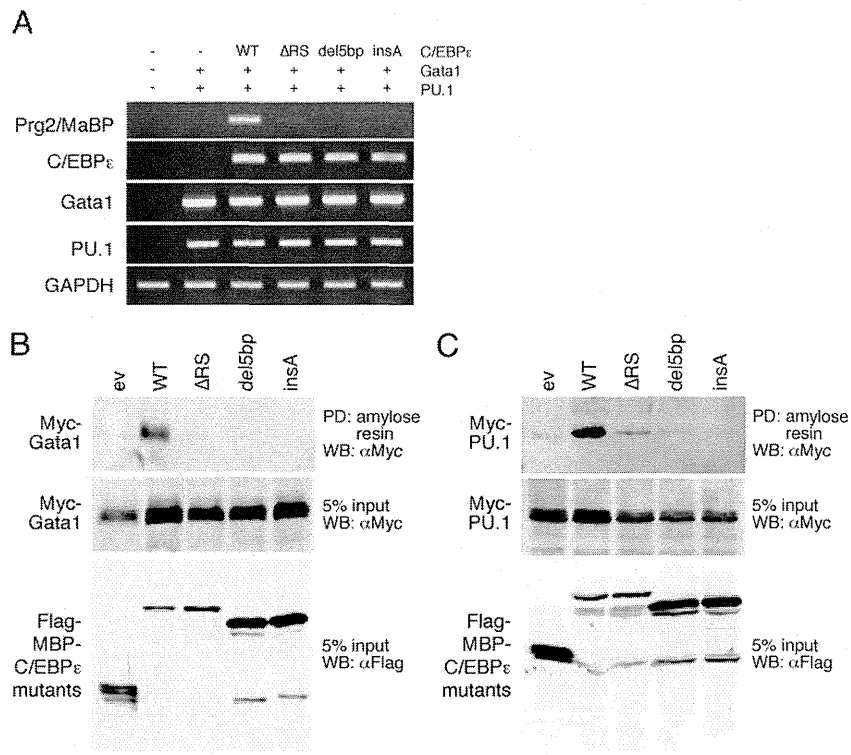

FIGURE 7. Cooperative transcriptional activation of eosinophil major basic protein (MaBP). (**A**) Induction of Prg2/MaBP expression in NIH3T3 cell. Expression vectors Gata1 and PU.1 were transfected into NIH3T3 cells either with or without C/EBPε expression vectors (WT, ΔRS, del5bp, or insA). Expression of endogenous Prg2/MaBP mRNA was examined by RT-PCR. GAPDH was used as a loading control. The numbers of PCR cycles were 20 for GAPDH, and 25 for C/EBPε, Gata1, PU.1 and MaBP. (**B** and **C**) Protein interactions between C/EBPε WT or mutants with either Gata1 or PU.1. HEK293 cells were transfected with either Myc-Gata1 or Myc-PU.1 together with an empty control vector (MBP-ev), Flag-MBP-C/EBPε-WT, -ΔRS, -del5bp, or -insA. MBP-fused proteins were pulled down by amylose resin, and the precipitates were analyzed by Western blot analysis with anti-Myc Ab. Expression of each protein was confirmed with anti-Myc and anti-Flag Abs, respectively.

are divided into two major subsets: $CD14^{++}CD16a^{-}$ and $CD14^{+}$ $CD16a^{+}$ cells. Various inflammatory conditions including infections lead to an increased subpopulation of $CD16a^{+}$ monocytes (20, 21). CD16 expression of neutrophils of patient P1 was associated with infections (data not shown); therefore, CD16a expression on SGD neutrophils may depend on inflammatory immune stimuli.

The reason why the patient's neutrophils expressed monocyte markers, including CD14 and CD16a, is presently unclear. Studies of granulocytes from healthy volunteers who were given G-CSF and from human embryonic stem cells treated with multiple growth factors have demonstrated aberrant expression of CD14 on mature granulocytes (22, 23). Although we did not measure any soluble factors related to granulocytic differentiation in our patients, defective myeloid differentiation in SGD could lead to dysregulated secretion of growth factors resulting in aberrant surface expression of neutrophil proteins. In vitro modeling of neutrophil development in SGD using induced pluripotent stem cells will be required to address these issues.

We carried out a comprehensive in vitro study to evaluate transcriptional activity, cellular localization, DNA-binding activity, dimerization and protein-interaction of the ΔRS mutant as well as the two frameshift mutants. All three mutants exhibited marked reduction in transcriptional activity. The ΔRS mutation is located in the bZIP domain, which is highly conserved among the C/EBP family members and has an important role in DNA binding and dimerization (5). However, the ΔRS mutant maintained normal cellular localization, DNA-binding activity, and dimerization, in contrast to the frameshift mutations del5bp and insA, which destroy the bZIP domain and thus are predicted to interfere with dimerization and binding to DNA. No dominant-negative effect of the ΔRS mutant may suggest that the single normal C/EBPε allele is sufficient to maintain transcriptional activity, which is consistent with the fact that the mother and two children of patient P1, who are assumed to be heterozygous for the ΔRS mutation, remain in good health. The association of C/EBPε with other transcription factors has been demonstrated to be important for the regulation of secondary granule gene expression in both neutrophils and eosinophils (15). In fact, the ΔRS mutant was found to be defective in association with Gata1 and PU.1, as well as aberrant cooperative transcriptional activation of eosinophil MaBP. Gata1 is primarily associated with erythroid and megakaryocyte differentiation, whereas PU.1 is more important for neutrophil differentiation. These results are in line with the fact that eosinophils were not detectable in patients P1 and P2. Taken together, our findings suggest that the ΔRS mutation impairs protein-protein interaction with Gata1 and with PU.1, resulting in loss of cooperative transcriptional activation.

A similar mutation has been described in a patient with acute myeloid leukemia, in which an in-frame 3-bp deletion within the leucine zipper domain of C/EBPα abrogated the transcriptional activation function of C/EBPα on the G-CSF receptor promoter (24). Like the ΔRS mutant, this mutant lacked a dominant-negative effect, although its protein-protein interaction with other transcription factors remained unexamined. Further investigation will be necessary to assess whether the ΔRS mutant also exhibits defective interaction with other transcription factors such as c-Myb, PML, p300, E2F1, and Rb (9, 16, 25, 26). Because certain isoforms of C/EBPε have been reported to inhibit the synergistic activities of GATA1 and PU.1 (25), we also need to evaluate the isoforms of the C/EBPε mutants other than the full-length, 32-kDa C/EBPε.

These characteristics of the ΔRS mutant, wherein modest association with Gata1 and PU.1 is retained and nuclear localization remains intact, may be associated with less severe clinical symptoms of patient P1. To date, patient P1 has shown no deep organ infection, whereas the other patients exhibited more severe presentation of the disease. The first reported patient with the del5bp mutation died of complications of pneumonia, and patient P2 suffered from recurrent pneumonia, as well as lung abscess (2, 3). On the other hand, recurrent bacterial skin abscess that persisted a few months was observed in all patients with SGD, including patient P1 (27). Skin abscess smears from patient P1 showed that most infiltrating cells were monocytes and macrophages, some of which phagocytosed bacteria (data not shown). Monocytes from C/EBPε-deficient mice exhibited impaired maturation and altered cytokine expression, such as increased levels of TNF-α and LTβ, in response to inflammation (28, 29). In addition, monocyte counts in C/EBPε-deficient mice were higher than those of WT mice (30). Thus, impaired inflammatory response and killing of bacteria by SGD patients' monocytes can hinder the healing process, resulting in unique skin abscesses. Understanding which factors evoke an abnormal microenvironment at infectious sites will be necessary to develop more effective therapeutic approaches for patients with SGD.

In summary, our studies identified a novel in-frame deletional mutation in the bZIP domain of C/EBPε and demonstrated its molecular pathogenesis leading to SGD. Comparative analysis of the C/EBPε mutations, including the previous frameshift mutations, also clarifies the functional significance of these mutants. Characterization of C/EBPε genetic defects and functional abnormalities will help to define the role of C/EBPε in human myelopoiesis and innate immunity.

Acknowledgments

We thank Dr. Kuniaki Naganuma for patient care and Harumi Matsukawa and Shizu Kouraba for technical assistance.

Disclosures

The authors have no financial conflicts of interest.

References

1. Gombart, A. F., and H. P. Koeffler. 2002. Neutrophil specific granule deficiency and mutations in the gene encoding transcription factor C/EBP(ε). *Curr. Opin. Hematol.* 9: 36–42.
2. Lekstrom-Himes, J. A., S. E. Dorman, P. Kopar, S. M. Holland, and J. I. Gallin. 1999. Neutrophil-specific granule deficiency results from a novel mutation with loss of function of the transcription factor CCAAT/enhancer binding protein ε. *J. Exp. Med.* 189: 1847–1852.
3. Gombart, A. F., M. Shiohara, S. H. Kwok, K. Agematsu, A. Komiyama, and H. P. Koeffler. 2001. Neutrophil-specific granule deficiency: homozygous recessive inheritance of a frameshift mutation in the gene encoding transcription factor CCAAT/enhancer binding protein—ε. *Blood* 97: 2561–2567.
4. Khanna-Gupta, A., H. Sun, T. Zibello, H. M. Lee, R. Dahl, L. A. Boxer, and N. Berliner. 2007. Growth factor independence-1 (Gfi-1) plays a role in mediating specific granule deficiency (SGD) in a patient lacking a gene-inactivating mutation in the C/EBPepsilon gene. *Blood* 109: 4181–4190.
5. Tsukada, J., Y. Yoshida, Y. Kominato, and P. E. Auron. 2011. The CCAAT/enhancer (C/EBP) family of basic-leucine zipper (bZIP) transcription factors is a multifaceted highly-regulated system for gene regulation. *Cytokine* 54: 6–19.
6. Chumakov, A. M., I. Grillier, E. Chumakova, D. Chih, J. Slater, and H. P. Koeffler. 1997. Cloning of the novel human myeloid-cell-specific C/EBP-ε transcription factor. *Mol. Cell. Biol.* 17: 1375–1386.
7. Lekstrom-Himes, J. A. 2001. The role of C/EBP(ε) in the terminal stages of granulocyte differentiation. *Stem Cells* 19: 125–133.
8. Yamanaka, R., C. Barlow, J. Lekstrom-Himes, L. H. Castilla, P. P. Liu, M. Eckhaus, T. Decker, A. Wynshaw-Boris, and K. G. Xanthopoulos. 1997. Impaired granulopoiesis, myelodysplasia, and early lethality in CCAAT/enhancer binding protein ε-deficient mice. *Proc. Natl. Acad. Sci. USA* 94: 13187–13192.
9. Verbeek, W., A. F. Gombart, A. M. Chumakov, C. Müller, A. D. Friedman, and H. P. Koeffler. 1999. C/EBPepsilon directly interacts with the DNA binding domain of c-myb and cooperatively activates transcription of myeloid promoters. *Blood* 93: 3327–3337.
10. Tang, J. G., and H. P. Koeffler. 2001. Structural and functional studies of CCAAT/enhancer-binding protein epsilon. *J. Biol. Chem.* 276: 17739–17746.
11. Shiohara, M., A. F. Gombart, Y. Sekiguchi, E. Hidaka, S. Ito, T. Yamazaki, H. P. Koeffler, and A. Komiyama. 2004. Phenotypic and functional alterations of peripheral blood monocytes in neutrophil-specific granule deficiency. *J. Leukoc. Biol.* 75: 190–197.

12. Toga, A., T. Wada, Y. Sakakibara, S. Mase, R. Araki, Y. Tone, T. Toma, T. Kurokawa, R. Yanagisawa, K. Tamura, et al. 2010. Clinical significance of cloned expansion and CD5 down-regulation in Epstein-Barr Virus (EBV)-infected $CD8^+$ T lymphocytes in EBV-associated hemophagocytic lymphohistiocytosis. *J. Infect. Dis.* 201: 1923–1932.
13. Sun, C., Y. Nakatake, T. Akagi, H. Ura, T. Matsuda, A. Nishiyama, H. Koide, M. S. Ko, H. Niwa, and T. Yokota. 2009. Dax1 binds to Oct3/4 and inhibits its transcriptional activity in embryonic stem cells. *Mol. Cell. Biol.* 29: 4574–4583.
14. Niwa, H., K. Yamamura, and J. Miyazaki. 1991. Efficient selection for high-expression transfectants with a novel eukaryotic vector. *Gene* 108: 193–199.
15. Gombart, A. F., S. H. Kwok, K. L. Anderson, Y. Yamaguchi, B. E. Torbett, and H. P. Koeffler. 2003. Regulation of neutrophil and eosinophil secondary granule gene expression by transcription factors C/EBP ε and PU.1. *Blood* 101: 3265–3273.
16. Gery, S., A. F. Gombart, Y. K. Fung, and H. P. Koeffler. 2004. C/EBPepsilon interacts with retinoblastoma and E2F1 during granulopoiesis. *Blood* 103: 828–835.
17. Uranishi, K., T. Akagi, C. Sun, H. Koide, and T. Yokota. 2013. Dax1 associates with Esrrb and regulates its function in embryonic stem cells. *Mol. Cell. Biol.* 33: 2056–2066.
18. McIlwaine, L., A. Parker, G. Sandilands, P. Gallipoli, and M. Leach. 2013. Neutrophil-specific granule deficiency. *Br. J. Haematol.* 160: 735.
19. Gery, S., D. J. Park, P. T. Vuong, D. Y. Chih, N. Lemp, and H. P. Koeffler. 2004. Retinoic acid regulates C/EBP homologous protein expression (CHOP), which negatively regulates myeloid target genes. *Blood* 104: 3911–3917.
20. Ziegler-Heitbrock, L. 2007. The $CD14^+$ $CD16^+$ blood monocytes: their role in infection and inflammation. *J. Leukoc. Biol.* 81: 584–592.
21. Mizuno, K., T. Toma, H. Tsukiji, H. Okamoto, H. Yamazaki, K. Ohta, K. Ohta, Y. Kasahara, S. Koizumi, and A. Yachie. 2005. Selective expansion of $CD16^{high}CCR2^-$ subpopulation of circulating monocytes with preferential production of haem oxygenase (HO)-1 in response to acute inflammation. *Clin. Exp. Immunol.* 142: 461–470.
22. Kerst, J. M., M. de Haas, C. E. van der Schoot, I. C. Slaper-Cortenbach, M. Kleijer, A. E. von dem Borne, and R. H. van Oers. 1993. Recombinant granulocyte colony-stimulating factor administration to healthy volunteers: induction of immunophenotypically and functionally altered neutrophils via an effect on myeloid progenitor cells. *Blood* 82: 3265–3272.
23. Yokoyama, Y., T. Suzuki, M. Sakata-Yanagimoto, K. Kumano, K. Higashi, T. Takato, M. Kurokawa, S. Ogawa, and S. Chiba. 2009. Derivation of functional mature neutrophils from human embryonic stem cells. *Blood* 113: 6584–6592.
24. Gombart, A. F., W. K. Hofmann, S. Kawano, S. Takeuchi, U. Krug, S. H. Kwok, R. J. Larsen, H. Asou, C. W. Miller, D. Hoelzer, and H. P. Koeffler. 2002. Mutations in the gene encoding the transcription factor CCAAT/enhancer binding protein alpha in myelodysplastic syndromes and acute myeloid leukemias. *Blood* 99: 1332–1340.
25. Du, J., M. J. Stankiewicz, Y. Liu, Q. Xi, J. E. Schmitz, J. A. Lekstrom-Himes, and S. J. Ackerman. 2002. Novel combinatorial interactions of GATA-1, PU.1, and C/EBPepsilon isoforms regulate transcription of the gene encoding eosinophil granule major basic protein. *J. Biol. Chem.* 277: 43481–43494.
26. Tagata, Y., H. Yoshida, L. A. Nguyen, H. Kato, H. Ichikawa, F. Tashiro, and I. Kitabayashi. 2008. Phosphorylation of PML is essential for activation of C/EBP ε and PU.1 to accelerate granulocytic differentiation. *Leukemia* 22: 273–280.
27. Roberts, R. L. 2014. Neutrophil-specific granule deficiency. UpToDate. Available at: http://www.uptodate.com/contents/neutrophil-specific-granule-deficiency.
28. Lekstrom-Himes, J., and K. G. Xanthopoulos. 1999. CCAAT/enhancer binding protein ε is critical for effective neutrophil-mediated response to inflammatory challenge. *Blood* 93: 3096–3105.
29. Tavor, S., P. T. Vuong, D. J. Park, A. F. Gombart, A. H. Cohen, and H. P. Koeffler. 2002. Macrophage functional maturation and cytokine production are impaired in C/EBP ε-deficient mice. *Blood* 99: 1794–1801.
30. Akagi, T., N. H. Thoennissen, A. George, G. Crooks, J. H. Song, R. Okamoto, D. Nowak, A. F. Gombart, and H. P. Koeffler. 2010. In vivo deficiency of both C/EBPβ and C/EBPε results in highly defective myeloid differentiation and lack of cytokine response. *PLoS ONE* 5: e15419.

J Clin Immunol (2015) 35:280–288
DOI 10.1007/s10875-015-0146-4

ORIGINAL RESEARCH

RAG1 Deficiency May Present Clinically as Selective IgA Deficiency

Tamaki Kato · Elena Crestani · Chikako Kamae · Kenichi Honma · Tomoko Yokosuka · Takeshi Ikegawa · Naonori Nishida · Hirokazu Kanegane · Taizo Wada · Akihiro Yachie · Osamu Ohara · Tomohiro Morio · Luigi D. Notarangelo · Kohsuke Imai · Shigeaki Nonoyama

Received: 10 November 2014 / Accepted: 17 February 2015 / Published online: 6 March 2015

Abstract
Background Recombination-activating gene (RAG) 1 and 2 deficiency is seen in patients with severe combined immunodeficiency (SCID) and Omenn syndrome. However, the spectrum of the disease has recently expanded to include a milder phenotype.
Objective We analyzed a 4-year-old boy who was initially given the diagnosis of selective immunoglobulin A deficiency (SIgAD) based on immunoglobulin serum levels without any opportunistic infections, rashes, hepatosplenomegaly, autoimmunity or granulomas. The patient was found to be infected with varicella zoster; however, the clinical course was not serious. He produced antiviral antibodies.
Methods We performed lymphocyte phenotyping, quantification of T cell receptor excision circles (TRECs) and kappa deleting recombination excision circles (KRECs), an analysis of target sequences of RAG1 and 2, a whole-genome SNP array, an in vitro V(D)J recombination assay, a spectratype analysis of the CDR3 region and a flow cytometric analysis of the bone marrow.
Results Lymphocyte phenotyping demonstrated that the ratio of CD4+ to CD8+ T cells was inverted and the majority of CD4+T cells expressed CD45RO antigens in addition to the almost complete lack of B cells. Furthermore, both TRECs and KRECs were absent. Targeted DNA sequencing and SNP array revealed that the patient carried a deletion of RAG1 and RAG2 genes on the paternally-derived chromosome 11, and two maternally-derived novel RAG1 missense mutations (E455K, R764H). In vitro analysis of recombination activity showed that both RAG1 mutant proteins had low, but residual function.
Conclusions The current case further expands the phenotypic spectrum of mild presentations of RAG deficiency, and suggests that TRECs and KRECs are useful markers for detecting hidden severe, as well as mild, cases.

T. Kato · C. Kamae · K. Honma · K. Imai · S. Nonoyama
Department of Pediatrics, National Defense Medical College, Tokorozawa, Saitama, Japan

E. Crestani · L. D. Notarangelo
Division of Immunology, Children's Hospital Boston, Harvard Medical School, Boston, MA, USA

T. Yokosuka
Department of Hemato-oncology/Regeneration Medicine, Kanagawa Children's Medical Center, Yokohama, Kanagawa, Japan

T. Ikegawa
Department of Pediatrics, Yokohama Rosai Hospital, Yokohama, Kanagawa, Japan

N. Nishida · H. Kanegane
Department of Pediatrics, University of Toyama, Toyama, Japan

H. Kanegane · T. Morio · K. Imai (✉)
Department of Pediatrics, Tokyo Medical and Dental University (TMDU), 1-5-45, Yushima, Bunkyo-ku, Tokyo 113-8519, Japan
e-mail: kimai.ped@tmd.ac.jp

T. Wada · A. Yachie
Department of Pediatrics, Kanazawa University, Kanazawa, Ishikawa, Japan

O. Ohara
Laboratory for Integrative Genomics, RIKEN Center for Integrative Medical Sciences, Yokohama, Kanagawa, Japan

O. Ohara
Department of Technology Development, Kazusa DNA Research Institute, Kisarazu, Chiba, Japan

Keywords *RAG1* deficiency · IgA deficiency · TRECs · KRECs · primary immunodeficiency · V(D)J recombination

Abbreviations

RAG	Recombination-activating gene
SCID	Severe combined immunodeficiency
SIgAD	Selective immunoglobulin A deficiency
TRECs	T cell receptor excision circles
sjKRECs	signal joint immunoglobulin kappa deleting recombination excision circles
cjKRECs	coding joint immunoglobulin kappa deleting recombination excision circles
PID	Primary immunodeficiency
RAGD	RAG deficiency
CVID	Common variable immunodeficiency
BMT	Bone marrow transplantation
LOH	Loss of heterozygosity
GFP	Green fluorescent protein
BM	Bone marrow
TCR	T cell receptor
FISH	Fluorescence in situ hybridization
BAC	Bacterial artificial chromosome
CID	Combined immunodeficiency
VZV	Varicella zoster virus
EBMT	The European Group for Blood and Marrow Transplantation

Introduction

Selective immunoglobulin A deficiency (SIgAD) is the most common form of primary immunodeficiency (PID) in the western world, affecting approximately 1/600 individuals, although there is marked variability in prevalence among different ethnic groups, with a lower frequency in Japanese (1/18,000) and Chinese (1/4,000) patients, thus suggesting a genetic basis for this disorder [1].

Complete *RAG* deficiency (RAGD) without a V(D)J recombination activity is associated with classical severe combined immunodeficiency (SCID) and the absence of T and B cells. Several clinical and immunological subtypes have been described in patients with hypomorphic *RAG* mutations, including Omenn syndrome (recombination activity of mutated RAG proteins: <1.5 % of normal) [2–4], leaky SCID (recombination activity 1.5–10 % of normal) [5], and RAGD with autoimmunity and/or granuloma (recombination activity: 10–60 % of normal) [6–10]. Engraftment of maternal T cells can add to the variation in phenotype [11].

We recently performed real-time polymerase-chain-reaction (PCR)-based quantification of TREC and signal joint immunoglobulin KREC for mass screening of SCID [12] and B lymphocyte deficiency [13] in neonates and to classify common variable immunodeficiency (CVID) [14]. T cell receptor excision circles (TRECs) and kappa deleting recombination excision circles (KRECs) are associated with T and B cell neogenesis, respectively.

In the present paper, we describe the case of a patient who was initially given the diagnosis of SIgAD based on immunoglobulin serum levels with absent TRECs and KRECs caused by *RAG1* mutations.

Patient, Materials and Methods

Patient

The patient was the first child of healthy Japanese parents with no consanguinity. At 4 years of age, he was hospitalized for pneumonia. He had no history of rashes or hepatosplenomegaly. Until that age, he had suffered from pneumonia once and otitis media twice. In addition, he had received standard immunizations including VZV vaccine at 4 years of age. He developed varicella 6 month after the first immunization, although the clinical course was not serious while taking oral aciclovir. Intracutaneous reactions to varicella was positive when tested at age 5, indicating that he had VZV specific T-cells at that time. He was initially given the diagnosis of SIgAD based on immunoglobulin serum levels at 4 years of age. (Table 1), and was found to produce antiviral antibodies including anti-VZV.

Flow Cytometric Analysis

The patient's peripheral blood mononuclear cells were analyzed using a FACSCalibur device (Becton Dickinson, USA).

Measurement of TRECs and KRECs

TRECs and KRECs quantification was performed using DNA samples extracted from the patient's peripheral blood, as previously reported [12, 13]. In the process of B-cell maturation, immunoglobulin kappa deleting recombination excision circles (KRECs) are produced during k-deleting recombination allelic exclusion and isotypic exclusion of the light chain. Coding joint (cj) KRECs reside within the chromosome, whereas signal joint (sj) KRECs are excised from genomic DNA. cjKREC levels remain the same after B-cell division, whereas sjKREC levels decrease, because sjKRECs are not replicated during cell division.

Sequence Analysis and Whole-Genome SNP Array

Peripheral blood mononuclear cells (PBMC) were isolated via Ficoll-Hypaque gradient centrifugation. $CD4^+$ and $CD8^+$ T cells and $CD19^+$ B cells were purified via positive selection

Table 1 Laboratory analysis, lymphocyte phenotyping and TRECs/KRECs at 4 years old and 6 years old (pre and post BMT). The intracutaneous reaction of varicella used a killed varicella, 5–10 mm of redness is normal range who has cellular immunity to varicella zoster virus

White cell count	4 years old	6 years old Pre HSCT	6 years old Post HSCT	Normal range	Specific antibodies	4 years old	Lymphocyte subgroup	4 years old	6 years old Pre HSCT	6 years old Post HSCT
Leukocytes (cells/μl)	4,600	7,000	3800	5500–15,500	EBV-VCA-IgG	+	$CD3^+$(%lymphocyte)	41.5	46.9	63.6
Lymphocytes (cells/μl)	598	560	646	2,000–8,000	EBV-VCA-IgM	−	$CD4^+$(%$CD3^+$)	37.1	31.3	35.9
Granulocytes (cells/μl)	2,116	4655	2812	1,500–8,500	EBV-EBNA	+	$CD8^+$(%$CD3^+$)	37.5	56.1	59.2
Monocytes (cells/μl)	230	420	114	500	CMV-IgG	−	$CD45RO^+$(%$CD4^+CD3$+)	98.0	94.1	88.2
Eosinophils (cells/μl)	1,564	1260	190	300	CMV-IgM	−	$HLADR^+$(%$CD4^+CD3^+$)	47.9	39.5	40.6
Immunoglobulin					VZV-IgG	+	$CD45RA^+CD31^+$(%$CD4^+CD3^+$)	0.8	1.3	9.3
IgG(mg/dl)	896	1096	1002	565–1,395	VZV-IgM	−	Treg CD127lo/- $CD25^+$(%$CD4^+CD3^+$)	9.4	6.5	4.1
IgA(mg/dl)	<5	1	2	29–190	Measles-IgG	+	$CD19^+$(%lymphocyte)	1.2	5.5	1.9
IgM(mg/dl)	122	45	27	78–315	Measles-IgM	−	$CD27^+$(%$CD19^+$)	40.1	50.6	47.5
IgE(IU/ml)	4	n.d.	n.d.	9.9–2200			IgM^+IgD^-(%$CD27^+CD19^+$)	23.7	15.2	4.7
IgG1(mg/dl)	637	n.d.	n.d.	390.5–1,289.8			IgM^-IgD^-(%$CD27^+CD19^+$)	47.4	5.43	72.6
IgG2(mg/dl)	152	n.d.	n.d.	106.4–381.9			NK(%lymphocyte)	40.3	20.5	19.0
IgG3(mg/dl)	5	n.d.	n.d.	12.8–92.5			γ/δ T(%$CD3^+$)	24.4	15.0	3.4
IgG4(mg/dl)	3.2	n.d.	n.d.	2.7–66.3			TRECs/KRECs			
T cell function							TREC(copies /μgDNA)	<100	<100	<100
PHA(cpm)	3430	n.d.	n.d.	26,000–53,000			cjKREC(copies /μgDNA)	<100	11400	7150
ConA(cpm)	2430	n.d.	n.d.	20,000–48,000			sjKREC(copies /μgDNA)	<100	<100	4850
Intracutaneous reaction of varicella	Redness 10 mm (++)	n.d.	n.d.	Redness ≤4 mm (−) 5–9 mm (+) ≥10 mm (++) ≥10 mm+ Induration (+++)						

from PBMCs using monoclonal antibody (mAb)-coated magnetic beads, according to the manufacturer's instructions (Miltenyi Biotec, Germany). DNA was extracted from blood samples obtained from the patient and his father, mother, brother and sister using standard methods. The *RAG1* and *RAG2* genes were amplified in several segments from genomic DNA using specific primers, as previously described. Sequencing of the purified PCR products was performed using the ABI Prism Big Dye Terminator Cycle sequencing kit on an ABI 3100 automated sequencer (Applied Biosystems, Foster, CA).

A copy number and loss of heterozygosity (LOH) analysis in the patient was performed using a CytoScan HD Array (Affymetrix, Santa Clara, California, USA), according to the manufacturer's protocol. The data were analyzed using the Chromosome Analysis Suite software program, v1.2. 0.225 (Affymetrix).

Fluorescence in situ hybridization (FISH) analysis was performed with bacterial artificial chromosome (BAC) clones, RP11-72A10 (11p12) and GS-44H16 (11p15.5).

In Vitro V(D)J Recombination Assay

The recombinase activity of the E455K, R764H mutations was explored using Abelson-immortalized murine Rag1$^{-/-}$tg.Eμ-bcl2 pro-B cells with an intrachromosomal inverted green fluorescent protein (GFP) cassette flanked by recombination signal sequences, as previously reported [15].

Flow Cytometric Analysis of the Bone Marrow (BM)

Heparinized samples of bone marrow were obtained from the patient. Following Ficoll-Hypaque centrifugation, the resultant mononuclear cells were fixed with 4 % paraformaldehyde (Wako Pure Chemical Industries, Ltd, Osaka, Japan) in PBS for 15 min at room temperature and then treated with 0.5 % saponin (Sigma) in staining buffer for 15 min on ice and thereafter was stained with PE-labeled anti-VpreB, PC5-labeled anti-CD19 mAbs and FITC-labeled antihuman μH chain Abs [16]. Then cells were analyzed using a FC500 (Beckman Coulter, K.K., Tokyo, Japan).

Assessment of T Cell Receptor (TCR) Diversity

The expression levels of the TCR Vβ families in the $CD4^+CD3^+$ cells and $CD8^+CD3^+$ cells were detected using the IO Test Beta Mark (Beckman Coulter, Brea, California). The TCRB repertoire was further investigated using CDR3 "spectratyping," that is, with a quantitative analysis of CDR3s of different sizes generated by the random insertion/deletion of nucleotides during V(D)J rearrangement, as previously reported [17]. A normal polyclonal repertoire results in a histogram with a Gaussian-like distribution of CDR3 lengths, whereas abnormal patterns display one or more predominant fragments outside the peak median length [17].

The study protocol was approved by the National Defense Medical College Institutional Review Board, and written informed consent was obtained from the parents of the patient in accordance with the Declaration of Helsinki.

Results

Lymphocyte Phenotyping, TCR Diversity and TRECs and KRECs Analysis

Because of the unusual clinical history as a SIgAD, we performed FACS and TRECs and KRECs analysis to define immunological phenotype of the patient. Immunophenotyping of the patient's PBMCs showed a low number of $CD4^+$T cells. The percentage of $CD4^+$ and $CD8^+$ T cells with a $CD45RO^+$ memory phenotype was strongly increased compared with that of $CD31^+$ naïve T cells. The TCR repertoire was moderately oligoclonal for $CD4^+CD3^+$ and $CD8^+CD3^+$ cells using flowcytometry (Fig. 3a) and a spectratype analysis of the CDR3 region of TCRVβ (Fig. 3b). In addition, B cells were almost completely absent at 4 years of age, although they were detected at 6 years of age, when IgM memory and switched memory B cells were also present (Table 1).

In addition, the levels of TRECs, cjKRECs and sjKRECs were undetectable indicated that T cells and B cells neogenesis were decreased or V(D)J recombination was impaired in the patient (Table 1).

Sequence Analysis and Whole-Genome SNP Array

Based on the FACS and TRECs/KRECs analysis, he was suspected of the combined immunodeficiency with developmental defect of T and B cells. Thus we performed DNA sequencing of *RAG1* and *RAG2* and found two novel and apparently homozygous missense mutations in *RAG1* (E455K, R764H) in PBMCs, $CD4^+$ T cells, $CD8^+$ T cells

Fig. 1 *RAG1* mutations. **a** DNA sequencing identified two apparently homozygous missense mutations in *RAG1* (*left*:c.1363G>A, *right*:c.2291G>A). Each cell subset of the patient was subjected to sequencing, which revealed no evidence of reversion mosaicism. **b** The SNP array analysis identified deletion of approximately 4 Mb extending from 11p12 to 11p13(chr11:34,401,525–38,380,493;hg19). **c** Non-mosaic heterozygous deletion of the 11p region was confirmed on FISH using BAC clones, RP11-72A10(11p12, *blue dot* with arrow) and GS-44H16(11p15.5, *red dot*). **d** Schematic representation of chromosome 11p with the deletion and *RAG1/RAG2* gene in the patient's paternally (P) and maternally (M) derived alleles. *tel* telomere, *cen* centromere. **e** Pedigree of the family

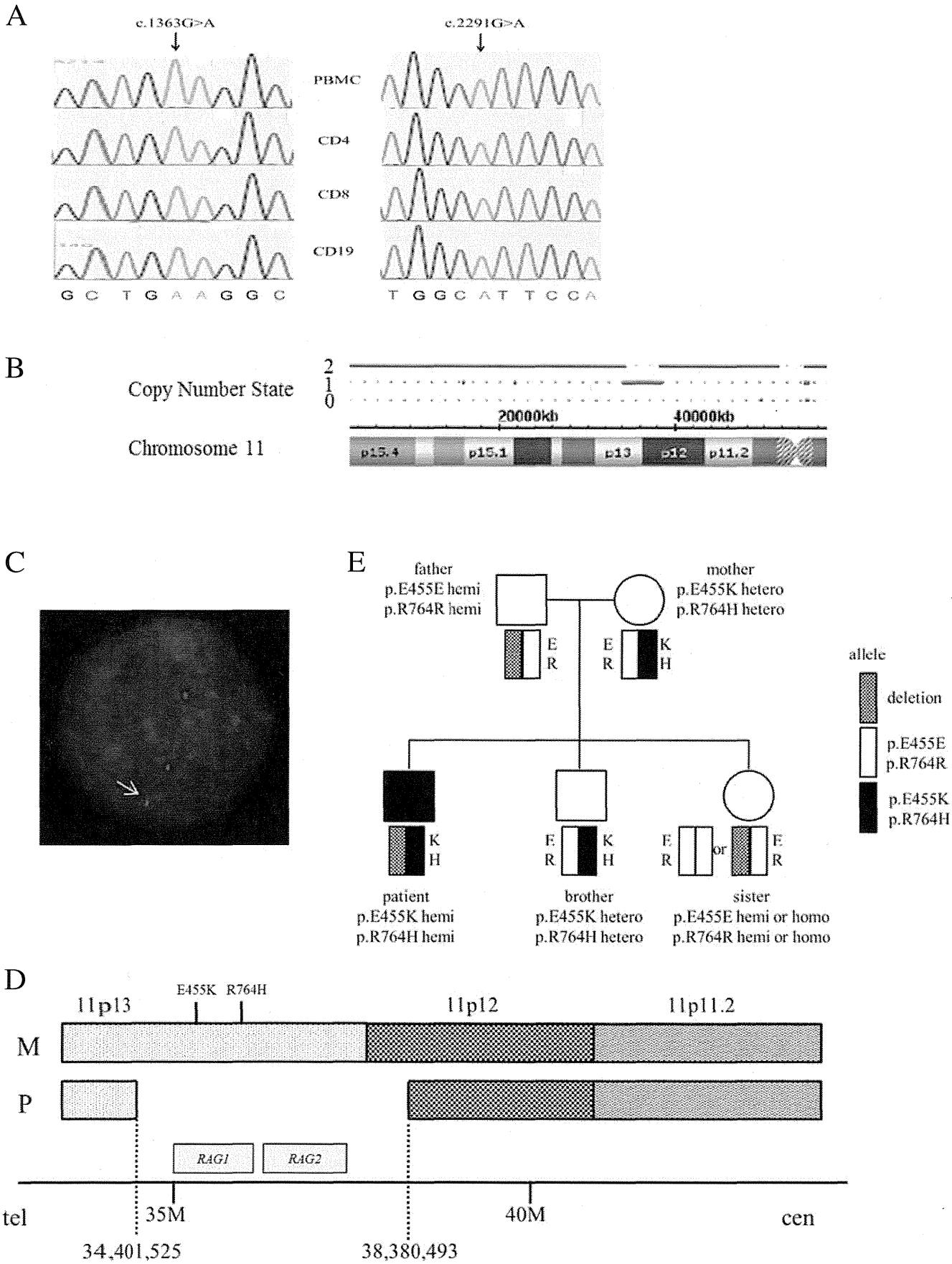
A
c.1363G>A
c.2291G>A
PBMC
CD4
CD8
CD19
G C T G A A G G C
T G G C A T T C C A
B
Copy Number State
Chromosome 11
2
1
0
20000kb
40000kb
p15.4
p15.1
p13
p12
p11.2
C
E
father
p.E455E hemi
p.R764R hemi
mother
p.E455K hetero
p.R764H hetero
E R
E K
R H
allele
deletion
p.E455E
p.R764R
p.E455K
p.R764H
K H
E K
R H
E or E
R R
patient
p.E455K hemi
p.R764H hemi
brother
p.E455K hetero
p.R764H hetero
sister
p.E455E hemi or homo
p.R764R hemi or homo
D
11p13
E455K R764H
11p12
11p11.2
M
P
RAG1
RAG2
tel
35M
40M
cen
34,401,525
38,380,493